

# **African Easterly Jet: barotropic instability, waves and cyclogenesis**

**Man-Li C. Wu\***

Global Modeling and Assimilation Office  
NASA Goddard Space Flight Center  
Greenbelt, Maryland 20771

**Oreste Reale †**

Laboratory for Atmospheres  
NASA Goddard Space Flight Center  
Greenbelt, Maryland 20771

**Siegfried D. Schubert, Max J. Suarez**

Global Modeling and Assimilation Office  
NASA Goddard Space Flight Center  
Greenbelt, Maryland 20771

**Chris D. Thorncroft**

Department of Earth and Atmospheric Sciences, University at Albany  
State University of New York, Albany, New York 12222

November 29, 2010

---

\*Email [Man-Li.C.Wu@nasa.gov](mailto:Man-Li.C.Wu@nasa.gov)

†Additional Affiliation: University of Maryland, Baltimore County, Baltimore, Maryland

This study investigates the structure of the African Easterly Jet focusing on instability processes on a seasonal and sub-seasonal scale, with the goal of identifying features that could provide increased predictability of Atlantic tropical cyclogenesis. The Modern-Era Retrospective analysis for Research and Applications (MERRA) is used as the main investigating tool. MERRA is compared with other reanalyses data sets from major operational centers around the world and found to describe very effectively the circulation over the African Monsoon region. In particular, a comparison with precipitation data sets from the Global Precipitation Climatology Project (GPCP) shows that MERRA produces the best seasonal precipitation over that region.

The verification of the generalized Kuo barotropic instability condition computed from seasonal means is found to have the interesting property of defining well the location where observed tropical storms are detected. This property does not appear to be an artifact of MERRA and is present also in the other adopted reanalyses data sets. Therefore, the fact that the areas where the mean flow is unstable seems to provide a more favorable environment for wave intensification, could be another factor to include, in addition to sea surface temperature, vertical shear, precipitation, role of Saharan air, and others, among large scale forcings affecting development and tropical cyclone frequency.

In addition, two prominent modes of variability are found based on a spectral analysis that uses the Hilbert Huang transform: a 2.5-6 day mode which corresponds well to the African Easterly Waves, and also a 6-9 day mode which seems to be associated with a tropical-extratropical interaction.

# 1. Introduction

This article investigates some large-scale properties of the atmospheric circulation over western Africa and the northern tropical Atlantic across seasonal and subseasonal time-scales, and particularly possible relationships between instability of the atmospheric flow, computed on a seasonal time scale, African Easterly Wave (AEW) activity and spatial distribution of tropical genesis points. The problem of tropical cyclogenesis can be studied from a variety of approaches, ranging from properties of the AEJ affecting wave development, intrinsic properties of the waves, mechanisms affecting the intensification of waves and actual occurrence of tropical cyclogenesis. It is widely accepted that sea surface temperatures (SSTs) and vertical shear are primary factors (e.g., Shapiro and Goldenberg 1998) controlling the genesis and development of tropical cyclones (TCs). In this article one additional factor, connecting the horizontal shear of the mean seasonal wind with regions of tropical cyclogenesis, is illustrated. Empirical Orthogonal Functions (EOFs) and a spectral analysis based on the Hilbert Huang transform (Huang et al. 1998; 1999) are used to separate purely tropical frequencies from modes that may represent some evidence of a tropical-extratropical interaction.

The research presented makes use of a synergistic approach involving spectral analysis, analysis of variance, composite analysis, and instability analysis. The article is a follow up of a previous study (Wu et al. 2009b, hereafter WA09) on the AEJ structure and on the mechanisms contributing to its maintenance. In WA09 the current understanding of the AEJ structure was discussed, as perceived

through state-of-the-art operational analyses, and a set of experiments aiming at understanding the forcing contributing to the AEJ structure and position. The results confirm in part previous findings by Thorncroft and Blackburn (1999), which emphasized the importance of low-level heating in controlling the AEJ, and by Cook (1999), which focused on the prominent role of soil moisture gradients. However, WA09 added new information by showing that it is not soil moisture alone that controls the AEJ position and structure, but rather a combination of forcings, among them soil moisture, vegetation properties, and orography, which appear to act together.

In this work, further research on the AEJ is presented, with a focus on mechanisms contributing to possible intensification of African Easterly Waves (AEWs) and to the spatial confinement of the TC genesis location points. The problem of TC formation is very broad and can be split into at least two parts: AEW production and AEW development into TCs. The problem of the formation of AEW is complex, especially if studied on the wave scale and investigating the internal structure of the waves (e.g., Kiladis et al. 2006; Hall et al. 2006). In particular, as an alternate and complementary view to the barotropic-baroclinic instability of the jet, waves can be studied from the point of view of internal triggering mechanisms (even without the contribution of the AEJ) by investigating the role of heating profiles (e.g., Thorncroft et al. 2008), of convection, and of vorticity structure on a subsynoptic scale. However, wave triggers and AEJ properties can work synergistically: Leroux and Hall (2009) show how convectively triggered waves are influenced by intraseasonal variability of the AEJ.

The problem of the development of AEWs into tropical cyclones is the subsequent logical step, and involves a variety of aspects depending on the scales of investigation. Sea surface temperature (SSTs) and vertical shear have been long considered as fundamental large-scale characteristics of the environment that influence tropical cyclone frequency. However, even having a hypothetical ‘perfect’ knowledge of these quantities, seasonal prediction of tropical cyclones would be limited. The importance of individual wave structures in influencing tropical cyclogenesis (e.g., Hopsch et al. 2010) is also recognized as one crucial aspect.

In this article, rather than focusing on the internal structure of individual waves and wave evolution, some additional large-scale properties of the flow across different time-scales and the effects of planetary-scale forcings are investigated. As will be shown, the results do not contradict previous well-established findings on large-scale mechanisms relevant for cyclogenesis, but rather add a new piece of information that may have implications on seasonal and subseasonal prediction capabilities.

The idea that some increase in tropical cyclone prediction skill on a subseasonal scale could derive from an improved understanding of the propagation of the equatorial circulation known as Madden-Julian Oscillation (MJO; Madden and Julian 1971, 1972) over the Pacific and Indian Oceans, has been intensely investigated (e.g., Leroy and Wheeler 2008). Given its powerful impact on a variety of atmospheric events across weather and climate scales (e.g., Asnani 2005), this is not surprising. The MJO can be conceived as an east-ward propagating disturbance characterized by active and inactive phases with enhanced and decreased

convective activity respectively. Even if this article does not discuss the MJO directly, several of the results obtained by MJO-related research are fully relevant to the problems addressed in this work, particularly to the subseasonal variability issue, and therefore need to be mentioned.

In particular, the mechanisms through which the MJO is believed to affect tropical cyclogenesis are not completely clear. For example, Maloney and Hartmann (2000b) found the MJO to cause changes in low-level vorticity and vertical shear over the eastern Pacific; however, Camargo et al. (2009) analyzed the modulation of TC genesis caused by MJO and detected the main mechanisms to be changes in low-level absolute vorticity and mid-level relative humidity, but only marginal contributions from vertical shear. Connections between the MJO and tropical cyclone processes have been observed and discussed for the eastern north Pacific (Maloney and Hartmann, 2000a), northern Pacific (Maloney and Hartmann 2001), the Australian region (e.g., Hall et al. 2001), the southern Indian Ocean (e.g., Bessafi and Wheeler 2006), and the southern Pacific (Chand and Walsh 2010).

Fewer studies however, have focused on the impact of the MJO on Atlantic tropical cyclogenesis appeared during the 25 years since the discovery of the MJO, probably because the MJO signal appears to be weaker over the Atlantic than over the Pacific or Indian Oceans (Shapiro and Goldenberg 1993). During the last years, however, some studies of the MJO's role in modulating TC activity in the Atlantic have been published. Among the first of these, Maloney and Hartmann (2000b) suggest a modulation of hurricane activity in the Gulf of Mexico by the

MJO. Aiyer and Molinari (2008) show an impact on tropical cyclogenesis in the Caribbean, Barrett and Leslie (2009) demonstrate a link between TC activity in the northern Atlantic and MJO, and the more recent work by Klotzbach (2010) discusses the relationship between Atlantic TC activity and MJO phases, the latter defined according to the definition of Wheeler and Hendon (2004).

One of the most important concepts (particularly for this study's purpose), coming out of several of these recent studies suggest that, in addition to the MJO signal being weaker over the Atlantic, the propagation and effects of the MJO over the African Monsoon and the Main Development Region (MDR, after Goldenberg and Shapiro 1996) seem to be strongly modified by the strength and sign of ENSO: in particular, Klotzbach (2010) argues that the ENSO signal needs to be removed in order to correctly ascertain subseasonal variability in the Atlantic. Kossin et al. (2010) do not limit their analysis to the MJO, but discuss the impact on tropical cyclone tracks caused by ENSO, the Atlantic Meridional Mode (AMM), the North Atlantic Oscillation (NAO), and the MJO, by utilizing a clustering technique previously applied to other basins. This provides a separation of four clusters of tracks, separated zonally and meridionally. The E-W separation corresponds to Gulf of Mexico versus Cape Verde system, whereas the N-S clustering separates 'purer' tropical systems from systems that display a higher degree of baroclinicity. The main impact of the MJO is found on the Gulf of Mexico systems.

The MJO is not discussed in this study; however, Klotzbach's (2010) argument on the need of removing the ENSO signal to better understand subseasonal

mechanisms is taken, and the effects of ENSO are removed by focusing only on ENSO neutral years.

A crucial tool for this work is the new Modern-Era Retrospective analysis for Research and Applications (MERRA, Bosilovich et al. 2006; Bosilovich et al. 2008) produced by the NASA Global Modeling and Assimilation Office (GMAO). The MERRA reanalysis is used in this study to investigate the AEJ, and is compared with reanalyses from other centers. Section 2 describes MERRA, the other data sets used for comparison, and the filtering methodology. Section 3 describes the climatology of the zonal wind and its gradients, as well as of precipitation. Section 4 describes some results of a spectral analysis. The spectral technique adopted here (Huang et al. 1998; Huang et al. 1999), to be described in the following section, has some advantages over conventional methods because it does not require assumptions on any periodicity. The results suggest that the commonly-used time window of 2 – 10 days can be divided into two sub-windows, confirming and revisiting previous findings by Diedhiou et al. (1998) and Diedhiou et al. (1999) but adding the new result that one of the two sub-windows appears purely tropical while the other provides some evidence of a tropical-extratropical interaction. Section 4 also provides an analysis of variance of some key fields that have been filtered in two time-windows, and discusses the implications of these results. Section 5 presents a dynamically-based discussion and interpretation of the findings, and states the conclusions.

## 2. Data and methodology

The MERRA data set was produced by the GMAO with a focus on improving the historical analyses of the hydrological cycle on a broad range of weather and climate time scales. As such, it serves to place the NASA Earth Observing System (EOS) suite of satellite observations in a climate context. The data assimilation and forecasting system used to produce the MERRA data is GEOS-5, documented extensively in Rienecker et al. (2008). In addition to the MERRA data this study uses: a) the ERA-40 reanalysis (Uppala et al. 2005) produced by the ECMWF for the period September 1957 to August 2002; b) the NCEP Department of Energy (NCEP-DOE) Reanalysis 2 (NCEP-R2, Kistler et al. 2001; Kanamitsu et al. 2002) which cover about thirty years; and c) the Japanese 25-year Reanalyses (JRA-25, Onogi et al., 2007). In this work however, only the data common to all the reanalyses (1980-2001) are used. All means, unless otherwise stated, are computed for the 1980-2001 period.

It is important to note that the reanalyses differ in resolution: the NCEP DOE data are at the lowest resolution: a triangular truncation at wavenumber 62 and 28 vertical levels (T62L28, corresponding to approximately 300 km or  $2.5^\circ$  horizontal resolution at the Equator), the JRA-25 data are at T106L40, which corresponds to approximately 190km or about  $1.5^\circ$ , the ERA-40 data are at T159L60 (horizontal resolution of about 125 km or about  $1.1^\circ$ ), and finally the MERRA products are at the highest resolution, of  $0.5^\circ \times 0.67^\circ$  and 72 vertical levels.

In addition to the reanalyses, the global monthly merged precipitation analy-

ses (1979-present) at  $2.5^\circ$  resolution from the Global Precipitation Climatology Project (GPCP, Adler et al. 2003) version 2.1 are used.

In this work, some filtering is performed on the data: in particular, a symmetric, 4-pole, low-pass, tangent Butterworth filter described in Oppenheim and Schaffer (1975), is applied to isolate temporal scales from 2.5 to 6 days and from 6 to 9 days. The particular choice of the time window, as will be shown later, is guided by the result of a Hilbert spectral analysis, following previous work by Huang et al. (1998), Huang et al. (1999), Wu et al. (1999), Huang and Shen (2005); and Wu et al. (2009a). The Hilbert-Huang transform produces a joint distribution of time-frequency-energy called the Hilbert Spectrum. The methodology, as discussed extensively in Huang et al. (1998, 1999), is adaptive, produces physically meaningful instantaneous frequencies as time differentials of the phase function, and is particularly suitable to analyze properties of nonstationary and nonlinear processes, since it does not require any assumption about oscillatory processes or particular wave functions. This is an important difference with respect to other techniques adopted to infer periodic properties of atmospheric motions.

### **3. Mean Climatology**

In Fig 1, the zonal wind climatology for July, August, and September (JAS) based on MERRA, is compared with that based on ERA-40, NCEP-R2, and JRA-25. The well-known structure of the AEJ and of the regional circulation can be distinguished in the four sets of reanalyses: in particular a jet maximum greater than

about  $11 \text{ m s}^{-1}$  is located at 600hPa at approximately  $15^\circ N$  over western Africa. As noted previously in WA09, the structure of the analyzed AEJ differs slightly on the eastern side, with NCEP-R2 extending it more to the east with respect to the others, and JRA-25 having the lower speeds over eastern Africa, and overall representing the weakest AEJ. The eastward extension of the AEJ, and its weakness particularly over data-sparse areas, such as the Ethiopian highlands, may be relevant to the development of AEWs in model forecasts (Agusti-Panareda et al. 2010). Among various minor discrepancies in the representation of the AEJ, it is noted that the ERA-40 and the NCEP-R2 products depict two distinct maxima in the AEJ (unlike MERRA which display one stronger elongated maximum), and the AEJ representation in MERRA and the ERA-40 extends more to the west than in the other two data sets. As pointed out in WA09, it cannot be argued, in the absence of a denser observational network (e.g., Parker et al. 2008), which of these representations of the AEJ is more realistic. The need of additional observations to further improve the representation of the AEJ, especially on its eastern side, has been stressed by many authors (e.g., Agusti-Panareda et al. 2010).

However, the different representations of velocity gradients in the different data sets is of greater interest than the simple assessment of the AEJ extension. To this purpose, the zonal wind structure with respect to the horizontal shear produced by the zonal component ( $u$ ) of the wind is also shown in Fig. 1. In particular, the two quantities  $\frac{-\partial u}{\partial y}$ , which is the relative vorticity associated with meridional variations in ( $u$ ), and  $K(y) = \frac{\partial}{\partial y}[f(y) - \frac{\partial u}{\partial y}]$  where  $f$  is the local Coriolis parameter, are superimposed.  $K(y) = 0$  represents the generalized Kuo

(1949) necessary condition for barotropic instability to occur in response to the zonal component of the flow.  $K(y) = 0$  on the cyclonic side of a flow indicates locations where barotropic instability is possible. If the flow is easterly, the condition favorable for barotropic instability in the northern hemisphere corresponds to a latitude  $y_{cr}$  where  $K(y_{cr}) = 0$  and  $K(y) > 0$  for  $y < y_{cr}$  and  $K(y) < 0$  for  $y > y_{cr}$ . In this work, we consider the range of values between  $-10^{-11}$  and  $10^{-11} m^{-1} s^{-1}$  to be sufficiently close to zero. So  $|K| < 10^{-11} m^{-1} s^{-1}$  delineate in this article the areas where the mean zonal component of the flow is unstable. Finally, in the left panels in Fig. 1 the areas where the vorticity induced by the zonal flow is cyclonic are shaded in white. The oceanic fraction of this region, constrained by the double condition of  $K$  being sufficiently small and the vorticity being positive, is also the area where most of the storm genesis points are observed, as will be shown later.

It is very significant that in all the reanalyses (less evidently in NCEP-R2) an area of negative  $K$  values is present at about  $15^\circ N$ ,  $20^\circ - 30^\circ W$ , which is the eastern edge of the MDR. In other words, the importance of this finding arises from the fact that in general one would regard the instability of the AEJ at any given time as an extremely complex issue, arising out of an instantaneous combination of both barotropic and baroclinic instability, as shown by Hsieh and Cook (2008) and previously discussed by Thorncroft and Hoskins (1994a; 1994b). The quantities involved in Fig. 1, such as horizontal shear  $\frac{\partial u}{\partial y}$  and  $K(y)$ , they also reflect the presence of baroclinic instability (e.g.,  $K(y) < 0$ ) and surface temperature gradients, but they are computed as a *time-mean* for the season. In addition, many

environmental factors such as sea surface temperatures, vertical shear, moisture and precipitation on various scales, contributions from Saharan Air, and cold air intrusions from the Mediterranean across the Sahara can all inhibit or enhance the development of AEWs into cyclones. Yet, the fact that something as simple as the barotropic instability of the *mean* flow, without considering any other property, appears to broadly coincide with the area where statistically a large amount of storms occur (being the Eastern border of the MDR), is important. The possible underlying reason is that where the AEJ is seasonally more unstable, there could be a higher probability that waves become more intense, and these in turn have a higher chance of producing tropical cyclogenesis. Again, without denying the importance of the many other factors that can affect tropical cyclogenesis, it is possible that the mean instability of the flow offers an additional constraint. If true, this would offer some potential for seasonal predictability, in that the mean flow is likely more predictable on a seasonal time-scale, than its higher frequency fluctuations.

As previously discussed, Fig. 1 shows some differences between reanalyses, such as that the analyzed AEJ and its gradients are stronger in MERRA than in the NCEP-R2 and JRA-25. On the other hand, the gradients and horizontal structure of the  $K(y)$  function at 600 hPa appear quite comparable in ERA-40 and MERRA, which indicate that the AEJ is more unstable in these data sets than in NCEP-R2 or JRA-25. It is also worth noting that the JRA-25 provides the less unstable representation of the AEJ particularly on its eastern side. These discrepancies could be partly caused by resolution, but also by different assimilation systems.

As seen Fig. 1, the stronger values of meridional shear of the zonal wind are concentrated in a strip to the south of the AEJ, receiving contributions from both easterly wind increasing with latitude, and westerly monsoonal flow to the south, and at lower elevations, decreasing with latitude. To further clarify this aspect, the vertical structure of the wind and gradients is illustrated in Figs. 2 and 3, where the corresponding meridional cross-sections of zonal wind,  $K(y)$  and meridional shear are plotted. Figure 2 emphasizes those heights and latitudes that are more barotropically unstable at a longitude of  $0^\circ$ . All four data sets agree that the strongest cyclonic shear induced by the AEJ is centered at about 600 hPa and slightly south of about  $15^\circ N$ , with the MERRA data displaying a more confined maximum. However, the cross-sections emphasize a different slope of the maximum shear values, that is even more evident in the  $K(y)$  plots. It is only MERRA and ERA-40 that display a clear ‘column’ of negative  $K$  values stretching from 900 to 500 hpa at about  $10^\circ - 15^\circ N$ .

Figure 3 shows the same meridional vertical cross-section at a longitude of  $20^\circ W$ , which intersects the region of interest completely over the ocean. The AEJ core is slightly to the north of  $15^\circ N$  in all reanalyses. Moreover, all cross-sections confirm the fundamental features of the AEJ and surrounding circulation consisting of: a low-level westerly flow confined below 800hPa and affecting the latitude band between the Equator and  $20^\circ$ , a low-level easterly flow (Harmattan) confined between  $20^\circ$  and  $30^\circ N$ , and an upper-level easterly flow (TEJ) at latitudes south of  $10^\circ N$ , with the MERRA data providing the stronger values. As seen in Fig 2, ERA-40 and MERRA consistently depict the cyclonically sheared

(southern) flank of the AEJ as barotropically unstable, with values of  $K(y)$  decreasing with increasing latitude, and with a near-zero  $K(y)$  vertical column even more vertically extended than at  $0^\circ$ , ranging from 900 hPa to almost 400 hPa. The implication is that the formation of a vertically aligned, barotropically unstable column seems to become even more likely as one moves from land ( $0^\circ$ ) towards the ocean ( $20^\circ W$ ). This is interesting because some developing waves tend to show vertically aligned structures at these levels when still over land, before transitioning from land to ocean, and even more so after transition since surface baroclinicity weakens over the ocean. The idea that waves grow out of a combination of baroclinic and barotropic instabilities over land, but that barotropic growth prevails over the ocean, is supported by several studies (e.g., Arnault and Roux 2009). Without denying that development occurs with many other contributing mechanisms, the fact that the mean seasonal flow displays some vertical alignment, which increases by moving from land to ocean, would suggest that a connection may exist between some instability properties of the seasonal flow and the individual systems. In other words, we are noting that mean properties of the flow seem to agree with requirements of individual systems, thus reinforcing the notion that a more unstable mean flow, more vertically aligned, is connected with the probability that individual systems may find a more favorable environment for development. At this time, this is a hypothesis to be further tested, but the preliminary evidence suggests that is plausible, and its implications are important.

It can be argued that the mean JAS climatological conditions reproduce in diluted form features that are observed often on weather time scales and instantana-

neous fields. As will be shown later, by comparing the locations where observed tropical cyclogenesis verifies, it seems that those areas where the *mean* flow satisfies the condition for barotropic instability on a seasonal time-scale are also the areas where actual storms cluster. At this time a connection cannot be strictly demonstrated, but it is worth noting that Hopsch et al. (2010) also note a tendency of genesis points to cluster towards the coastal area, and attribute the clustering of coastal developments to increased vorticity induced by rainfall over the Guinea highlands.

Figure 4 shows the precipitation climatology, together with the departures from the GPCP data sets. As is to be expected with the larger uncertainties typical of precipitation fields, the differences between reanalyses are large, with ERA-40 and NCEP-R2 having a wet bias on the southern side of the ITCZ, MERRA having a dry bias on the northern side of the ITCZ and to the east, and JRA-25 having a wet bias over the Sahel and a dry bias over the Guinea coast. In terms of absolute differences, it should be noted that the MERRA data set has the overall smallest departure from GPCP: less than  $3 \text{ mm d}^{-1}$  over most areas, and a mean departure of only  $0.04 \text{ mm d}^{-1}$  against  $1.48$ ,  $0.74$  and  $1.0 \text{ mm d}^{-1}$  for ERA-40, NCEP-R2, and JRA-25, respectively. However, MERRA has the largest dry bias over the east, which may indicate, according to Thorncroft et al. (2008), a lower number of AEWs being triggered. In the same figure, the variance of the interannual precipitation departures from the JAS GPCP mean is computed for all the four reanalyses sets throughout the 1980-2001 period. It is important to note that the variance of the difference with GPCP is the smallest for MERRA (1.92, against

the largest being 4.9 for ERA-40). The variance, together with correlation (not shown), is an indicator suggesting that interannual variability is represented well in the MERRA data set.

#### **4. Spectral analysis and analysis of variance**

As stated previously, to avoid contamination by the ENSO signal, which needs to be removed (e.g., Klotzbach 2010) to properly understand the mechanisms involved, an EOF analysis is performed across the ENSO neutral years on the meridional component of the 700 hPa wind, in the time window ranging from 2.5 to 90 days. The EOFs are computed on a domain ranging from  $40^{\circ}W$  to  $10^{\circ}E$  and  $10^{\circ}N$  to  $20^{\circ}N$ . Zonal changes in the domain within the same latitude range do not show major impact on the EOF structure (not shown). Figure 5 shows the first two principal components (PCs) resulting from this analysis: these account for about 40% of the total variance. The two EOFs are in quadrature and explain a comparable amount of variance, thus providing a representation of propagating easterly waves. The third and fourth EOF each account for an additional 11% of the variance (not shown), so that the first four components explain about 62% of the total variance.

The Hilbert Huang spectra were preliminary computed for the first four PCs over the entire domain and sub-domains (not shown). The frequencies at which peaks of spectral density occur are an indication of physically meaningful instantaneous periodicities (Huang et al. 1998; 1999) suggesting dominant time-scales of atmospheric motion. The results from this preliminary calculations hinted at an

interesting property: time scales greater and smaller than 6 days appeared to be separated in the first two EOFs (with two peaks at about 6.5 and 5 days respectively), but not on the third EOF and fourth EOF (not shown). In addition, spectra computed on different sub-domains seemed to suggest that the two time scales of atmospheric motion, separated by the 6 day period in the first two EOFs, appeared to dominate in different locations (as will be discussed later), with the time scale smaller than 6 days confined at the lower latitudes and the time scale greater than 6 days more prominent in the subtropics (not shown).

Based on these preliminary assessments, and to substantiate this aspect further, the Hilbert Huang spectra are shown for two locations, north and south of the AEJ axis respectively, at  $17^{\circ}W$  and  $12^{\circ}N$  and  $5^{\circ}W$  and  $26^{\circ}N$  and compared with the corresponding Fourier analyses. These locations are chosen because of their representativeness: the former refers to a point slightly south of the AEJ core, immediately off the west coast of Africa, the latter refers to a point north of the AEJ, over land. In Fig. 6 the Hilbert-Huang and Fourier spectra for the meridional component of the 700hPa wind are presented, for the point at  $17^{\circ}W$  and  $12^{\circ}N$ . The abscissa indicates frequency in terms of number of cycles over the length in days  $n$  of the JAS period, whereas the ordinate indicates spectral density.

Unlike the spectral analysis previously computed on the EOFs, in Fig. 6 the Hilbert-Huang transform is performed on the full field. A prominent sharp maximum at approximately  $10^{1.91}/n$  (about 5 days), between two minima that correspond to approximately periods of 2.5 and 6 days, indicates the most prevalent frequency of AEWs according to the Hilbert-Huang spectral analysis. Another,

less sharp and broader maximum at about  $10^{1.1}1/n$  indicates an oscillatory mode of about two or three weeks, which appears westward propagating (not shown), and therefore different from the quasi-stationary mode observed by Mounier et al. (2007) but similar to the periodicity of 10-30 days discussed by Janicot et al (2010). Other time scales greater than a month are also present but are not central to this article.

Figure 7 is the same as Fig. 6, except the Hilbert-Huang spectra are computed for a location over the Sahara, to the north of the AEJ and more to the East, at  $5^{\circ}W$  and  $26^{\circ}N$ . Spectra computed for locations at the same latitude but on the ocean ( $20^{\circ}W$ ) are very similar (not shown). In the Hilbert-Huang spectra, there is clear evidence of the same maximum at about  $10^{1.9}1/n$  confined by the time-scale of 2.5-6 days, but also of another maximum at about  $10^{1.3}1/n$  which is the center of the time-scale window of 6-9 days. This maximum does not appear in the Fourier spectrum. It is important to emphasize that the Hilbert Huang transform does not need any assumption on specific sinusoidal functions as the Fourier transform, and as such it is more likely to represent physically meaningful time scales. Since in this data set the 6-9 mode appears undetected when performing the Fourier analysis, it is possible that the preferred use of Fourier transform by several authors has been one of the reasons why the 6-9 time scale has received less attention. However, African waves with time scales of 6-9 days were observed and studied by De Felice et al. (1990, 1993), and previously by Yanai and Murakami (1970), who performed spectral analyses of equatorial waves and noted westward propagating disturbances over northern Africa with periods of about a week. As will be

discussed later in Section 5, in this work the 2.5-6 day frequency range appears to be connected with AEWs, whereas the 6-9 day seems to be produced by an interactions of tropical disturbances with midlatitude variability. Possible causes for this time scale will be discussed later in this Section and in Section 5.

Since this study is mostly focused on the seasonal-mean instability properties of the AEJ, and its possible link to weather systems, the variance of the meridional component of the wind is used to assess AEW activity and more generally increased activity, since large convective systems are also associated with increased variance of the wind (Fig. 8). However, considering the resolution of reanalyses, and their inability to resolve unorganized convective systems, it is likely that the wind variance reflects predominantly AEW activity. The most striking element in Fig. 8 is the overlap between the areas of maximum fraction of total variance and the areas where  $K(y)$  is close to zero (within the interval  $-10^{-11}$  to  $10^{-11}m^{-1}s^{-1}$ ). The maximum variance more to the north is associated with areas where  $K(y) < 0$  (recall Fig. 1) and with baroclinic instability. As stated before,  $K(y)$  is computed from the JAS average, and it represent the *areas where disturbances are more likely to extract kinetic energy from the mean zonal flow by barotropic growth*, in addition to the combined effect of baroclinic growth caused by negative potential vorticity gradients in the jet core (dominated by  $K(y) < 0$ ) and positive surface temperature gradients which are strong over land. The fact that this area coincides well with the areas where the variance of the meridional wind (indicative of actual wave activity computed from daily data and filtered on wave time-scales) is maximum, is remarkable. This suggests that instability properties of the mean flow

are connected with instabilities occurring on the instantaneous flow. If substantiated by further results, this relationship would provide a powerful diagnostic tool to assess the potential for AEW development and tropical cyclone genesis within seasonal forecasting runs. It is important to stress that no obvious correspondence between seasonal means of large scale fields and occurrence of individual storms has been found in other basins such as the Indian Ocean, for example, where storm genesis and development is extremely erratic. On the contrary, it appears that the Atlantic tropical cyclogenesis has a higher degree of constraint than other basins and, as such, may offer larger room for predictability on a seasonal scale.

In Fig. 9, the same plot is produced from precipitation data sets, to further support the point above. The 2.5-6 day band-pass filtered precipitation south of the AEJ is a strong indicator of wave activity and/or enhanced convection. It should be noted that a good correspondence exists between the maximum filtered precipitation variance and the areas that, in Fig. 8, display a correspondence between variance of meridional wind and areas where the mean flow satisfies the barotropic instability condition (and of baroclinic where  $K(y) < 0$ ) on a seasonal time scale. This correspondence is not an artifact of MERRA but is qualitatively present also in the other reanalyses (not shown).

In Fig. 10, the 2.5-6 day band-pass filtered variance of the zonal and meridional wind components, computed from MERRA at 500, 600, 700, 850 and 925 hPa, emphasizes the three-dimensional structure of the variance, and also shows the levels which are more active on this time-scale. It is important to look at the different behavior of both zonal and meridional components, to investigate wave

activity and possible energy exchanges between the jet and waves. The variance of the zonal component has a distinct maximum at about  $10^{\circ} - 15^{\circ}N$  and 600 hPa, whereas the variance of the meridional component is stronger at about  $15^{\circ}N$  and 925 hPa. It is significant that the variance of the meridional component, which suggest stronger disturbances and enhanced convection, peaks at the lower levels, right at the transition from coast to ocean in agreement with Hopsch et al (2010) findings. This may indicate that, in the reanalyses fields, the low-level meridional amplitudes may form once disturbances originating at the AEJ level (evident in the zonal fields in Fig. 10) reach the coastline and will in turn activates the amplitudes of the meridional component, which manifest themselves more clearly in the lower levels. The peak in the variance of the meridional component at 925 hPa is also consistent with the contribution to wave growth caused by surface baroclinicity.

It is very important to stress that this is not an artifact of the particular assimilation and forecast system adopted: exactly the same result, notwithstanding minimal internal differences, is also obtained by computing the same quantities from the ERA-40, NCEP-R2 and JRA-25 reanalyses (not shown). In fact, all four reanalyses show, over the ocean, a maximum of the 2.5-6 day filtered variance of the zonal wind component at 600 hPa, and a maximum of the 2.5-6 day filtered variance of the meridional wind component at 925 hPa. This is an indication of a fundamental property of the flow and its tendency to produce, or strengthen, disturbances that grow both barotropically and baroclinically. However, over land, JRA-25 shows much less variance, consistent with the overall weaker AEJ shown

in Fig. 1 and with the lower resolution.

Figure 11 shows the same fields as in Fig. 10, except that the winds are filtered to retain 6-9 time scales. The intent of this figure is to shed some light on the spatial distribution of this mode, and ascertain whether it is purely tropical or rather results from interaction with higher latitudes. The figure shows that the 6-9 time scales of motion do not produce a strong signal in the lower latitudes and lower levels. On the contrary, most of the signal of 6-9 day zonal wind is at 600-700 hPa, with a shape that is surprisingly similar to the typical track of early recurving disturbances. For the bandpass filtered meridional component, there is a maximum only north of  $20^{\circ}N$  at levels higher than 700 hPa, including 500 hPa. The shape of this maximum is surprisingly similar to the common ‘plumes’ of moisture advected by a predominantly southwesterly flow, which are often seen in water vapor channels stretching from the Atlantic ITCZ towards the northeastern Atlantic or the Mediterranean region (e.g Turato et al. 2004).

As stated before, time scales of 6-9 days, based on single point observations, were noted and documented by De Felice et al (1990, 1993). However, not being able to reproduce this as a global equatorial mode in a theoretical modeling framework, the authors concluded that the monsoonal signal might hide the signal in the Pacific and Indian oceans (De Felice et al. 1993). However, Diedhiou et al (1998) and Diedhiou et al. (1999) confirm the presence of the 6-9 mode but note that it appears at a more northern latitude, it is less intense in June-July and attribute it to periodic strengthening of subtropical anticyclonic cells. In this study, we suggest an explanation for the 6-9 mode different by De Felice et al. (1990, 1993),

and involving an interaction with extratropical dynamics and more in line with the findings by Diedhiou et al. (1998; 1999). In particular, we suggest that the 6-9 day filtered variance may indicate a very complex tropical-extratropical interaction between midlatitude and tropical activity. Of this interaction, more than one possible connected category of events could be symptoms: for example, tropical systems that recurve earlier and turn into northward or eastward motion, or the southernmost edge of fronts connected with the midlatitude activity. These are connected because a relaxation of the high pressure belt at about  $20^{\circ}N - 30^{\circ}N$  often allows the southern edge of fronts to penetrate further south and, at the same time, drive southerly flow ahead of such cold fronts away from the deep tropics into the midlatitudes. Disturbances originating from AEWs can frequently be advected northward in such flow at various levels of development, being either convective clusters which end up feeding the warm sector of midlatitude cyclones, or tropical systems commonly known as ‘early recurvers’ that are steered by a mid-level southwesterly flow, and different therefore from those Cape Verde systems which cross the Atlantic towards the American continent. Contributions of moist tropical air following trajectories very similar to the patterns shown in Fig. 11 have been found to be significant for floods in the Mediterranean region (e.g. Reale et al. 2001; Turato et al. 2004, Krichack et al. 2004).

To further emphasize the physical foundation of separating the spectrum in the two sub scales, Figure 12 shows the variance of the 700 hPa meridional component of the wind filtered through a 2.5-9 day, 2.5-6 day and 6-9 day passband respectively. There is a clear spatial separation between the two sub windows,

with the 6-9 day mostly confined at latitudes higher than  $20^{\circ}N$ . An almost identical result is obtained when plotting the same quantities from ERA-40, NCEP-R2 and JRA-25 (not shown), suggesting a robust physical foundation for the idea that two separate time-scales seem to be present over the region. At the same time, some variance in the 2.5-6 day passband at about  $20^{\circ}N$ , although weaker than the main peak confined at about  $20^{\circ}N$ , supports the idea that the 2.5-6 day mode weakens with the increase in latitude.

In Figure 13 the lag-correlation coefficient computed between the 700hPa zonal and meridional components of the wind at one location ( $20^{\circ}W$  and  $26^{\circ}N$ ) and all the surrounding points, at lag intervals of one day, is shown. The Figure illustrates what appears to be a mode propagating on a time scale of about 7 days and centered in the transitional zone between the deep tropics and the extratropics. It appears to be a physically based motion structure, founded on the interaction between midlatitude activity and tropical dynamics. That the ITCZ periodically breaks and reforms and that pulses of enhanced and reduced organized convection unrelated with AEW activity are observed in that latitude range is known to operational weather forecasting in the tropical Atlantic: with this work it is suggested that this is more than chaotic variability but that it may be the result of the interaction between midlatitude activity and tropical dynamics. Over the African monsoon region and the tropical Atlantic, cold air outbreaks are observed on a regular basis (e.g. Vizy and Cook 2009) in the forms of cold surges associated with shortwave trough passages over the Mediterranean Sea. These cold surges enhance convection over northern and western Africa but reduce it over the

eastern Sahel. It is possible that the particular topography of northern Africa and the Mediterranean Sea favors some tropical-extratropical interaction with a well-defined time-scale, that this interaction is captured by the Hilbert-Huang analysis, but has not received recent attention since the article by Diedhiou et al. (1999). This periodicity is different from the larger time scales studied by Janicot et al. (2010) and appears to be a little-known phenomenon that can potentially affect the way in which AEWs and midlatitude troughs interact.

We finally substantiate the importance of a) stratifying the analysis of the dynamics on the region according to the ENSO sign, and b) emphasizing the physical meaningfulness of both the 2.5-6 day bandpass filtered 700 hPa variance of the meridional wind and the low values of mean  $K(y)$ . The need of filtering out the ENSO signal to better understand the circulation over the region was emphasized by several authors including Klotzback (2010). In this article we focus on ENSO neutral years. Since the AEJ properties are different in the positive or negative ENSO years (not shown here), a treatment of the behavior of the AEJ in response to the ENSO signal will be the subject of a following article. Figure 14 shows the variance of the meridional wind, the genesis points of observed storms and the area characterized by near-zero  $K(y)$  values, all overlaying the mean zonal wind climatology in neutral ENSO years. It is worth observing the areas over the ocean where the variance is a maximum, plotted only within the areas where  $K(y)$  is in the range between  $-10^{-11}$  and  $10^{-11} m^{-1} s^{-1}$  correspond well with the portion of the eastern Atlantic ocean where tropical cyclogenesis occurs. In other words, a clear link appears to exist between 2.5-6 day filtered variance of the meridional

component of the 700 hPa wind, the satisfaction of barotropic instability condition for the mean zonal wind, and the occurrence of observed developments of tropical systems. The above link does not appear in the positive or negative ENSO years, possibly because of the way in which ENSO impact affect, among other factors, the vertical shear. The discussion on ENSO will be the subject of a future article.

## **5. Discussion and concluding remarks**

This article starts with an analysis of the AEJ using MERRA data, and comparing the AEJ representation with that in other reanalysis data sets, namely ERA-40, JRA-25 and NCEP-R2. The comparison has demonstrated the value of MERRA data as a tool for analyzing the African monsoon region, and on examining those aspects of the African Easterly Jet that may be relevant to the seasonal predictability problem.

It was shown that while discrepancies between reanalyses in the representation of the circulation over Africa are getting progressively smaller with respect to previous studies (i.e., Cook 1999), some differences still exist, and these differences are likely due to insufficient data coverage or to the response of different model physics in the absence of data. Despite these small differences in the representation of the AEJ, the reanalyses agree on the fact that the cyclonically-sheared flank of the AEJ has some properties, discussed later in the article, that may be important in increasing seasonal forecasting skill. This is a hypothesis that needs to be further investigated, but the preliminary results of this study are encouraging.

An assessment of the mean JAS precipitation shows that MERRA produces

the smallest bias with respect to GPCP compared with other reanalyses (Fig. 4). Soil moisture gradients, a prominent factor controlling the AEJ, are difficult to assess and verify; however the overall quality of precipitation distribution in the MERRA data appears satisfactory.

A Hilbert-Huang spectral analysis performed on the data sets reveals that two fundamental time scales can be recognized: at 2.5-6 days, consistent with the variability associated with AEWs, and a variability at 6-9 days. The latter is consistent with a 6-9 day propagation mode discussed by Yanai and Murakami (1970), De Felice et al. (1990), Diedhiou et al. (1998) and Diedhiou et al. (1999). However, this mode of variability did not receive as much attention within the scientific community as the 3-6 day time scales, possibly because of its more elusive signal, which our study suggests to be better captured by using the Hilbert Huang transform (Fig. 7). In this study we hypothesize that the mode is not purely tropical, as thought by De Felice et al. (1990), because we detect its signal more clearly at more northerly latitudes, in agreement with Diedhiou et al. (1998). Diedhiou et al. (1999) attribute the oscillation to periodic strengthening of the subtropical highs, without searching for a more northern origin. In this article, we speculate instead that the 6-9 mode may arise as a result of a tropical-extratropical interaction. In particular, we note the similarity of the 6-9 day filtered variance of the zonal component of the wind in the levels between 500 and 700 hPa with the typical track of 'early recurvers', and the substantial high latitude of the maximum 6-9 band-pass filtered variance of the meridional component of the wind, reminiscent of the tropical moisture plumes sometimes advected within the southern edge of certain

midlatitude disturbances.

These could be symptoms of a larger scale oscillation, such as the previously observed mode of 6-9 days (Yanai and Murakami 1970). However, the spatial distribution evidenced by the spectral and analysis of variance in this work allows to speculate that Yanai and Murakami (1970) perhaps incorrectly attributed the 6-9 time scale to an equatorial oscillation. The 6-9 periodicity may be instead an indication of either a subtropical oscillation, or of a tropical-extratropical connection, possibly arising out of the periodic weakening of the descending branch of the Hadley cell coincident with the transit of midlatitude frontal systems north of  $30^{\circ}N$ , which in turn causes a temporary relaxation of the ITCZ. This allows enhanced southwesterly moist flow advected in the the lower mid-troposphere (as seen in Turato et al. 2004) from the deep tropics ahead of midlatitude cold fronts, and cooler northerly flow in the lowest levels on the rear of them (as documented in Vizi and Cook 2005). It is worthy noting that Diedhiou et al. (1999) explanation of the 6-9 mode as resulting from the subtropical height strengthening is not inconsistent with the reasoning suggested in this work: if an extra tropical system transits north of a subtropical high, a ridging tendency with consequent subtropical high strengthening can be observed ahead of the midlatitude system, and a weakening to the rear of it, consequent to cooler northerly low-level flow advection. The 6-9 periodicity may then coincide with a strengthening (and weakening) of the subtropical anticyclones (as suggested by Diedhiou et al. (1999)) caused by an interaction between tropical and extratropical dynamics, or by a 'subtropical oscillation'.

In this article it is also noted that the necessary condition for barotropic instability computed from the JAS mean zonal wind delineates an area where the variance of the bandpass filtered (in the 2.5-6 day window) meridional component of the wind has a strong maximum. The maximum also corresponds well with the bandpass filtered precipitation variance maximum (Fig. 9), consistent with the fact that increased variance of the meridional component indicates increased wave activity or increased convection.

Finally the same area where the necessary condition for barotropic instability is satisfied in the above sense (being  $|K| < 10^{-11} m^{-1} s^{-1}$ ) is also the area where, during ENSO neutral years, observed formation of tropical storms occurs (Fig. 14). This is significant because the actual process that can transform an AEW into a closed circulation, is described in much more complicated terms by a combination of barotropic and baroclinic instabilities of the Charney-Stern kind (e.g. Thorncroft and Hoskins 1994a; Hsieh and Cook 2005). Additional degrees of complexity are introduced by thermal vertical structure (Thorncroft et al. 2008), convection, vorticity and moisture distribution (e.g. Hopsch et al. 2010) and with the crucial contribution of other factors such as sea surface temperatures, vertical shear and Saharan air intrusions. Yet, barotropic instability alone, when computed from the seasonal mean zonal wind, appears to strongly constrain the locations where storms occur. Further investigation on the interannual variability is needed, but if this preliminary finding is confirmed by future studies, it appears as a potential predictor of TC genesis on a seasonal scale.

In conclusions, there are two major findings that arise from this study.

- The verification of the Kuo barotropic instability condition, and of  $K(y) < 0$ , computed from the mean JAS zonal wind, has a physical meaning because it outlines very well the areas where storm genesis occurs.
- A Hilbert-Huang spectral analysis reveals two prominent modes of variability: one at 2.5-6 days, which corresponds to AEWs, and the other at 6-9 days, which appears to be connected with tropical-extratropical interactions or with a sub-tropical oscillation.

A caveat should be inserted. In this article, only seasonal means of the properties of the cyclonically-sheared flank of the AEJ have been shown. To verify if these properties have a true meaning in the predictability problem, the inter-annual variability of the AEJ properties and the vorticity sign reversal should be investigated. To do so, however, leads to the problem of discussing the role of ENSO which is not a goal of this article. Therefore, the possibility of the seasonal properties of the flow affecting development of individual waves is presented as a working hypothesis. This paper acknowledges the overall complexity of extended-range tropical forecasting in the Atlantic, but suggests a direction in which efforts could go, by connecting properties of the monthly mean flow with tropical cyclogenesis, and by suggesting a stratified approach that separates ENSO neutral years from the ENSO positive or negative years. An extended treatment of the ENSO signal on Atlantic tropical cyclogenesis will be the subject of a subsequent article.

**Acknowledgments** This work was supported by the NASA Earth Science En-

terprise's Global Modeling and Analysis Program.

## REFERENCES

- Adler, R.F., G.J. Huffman, A. Chang, R. Ferraro, P. Xie, J. Janowiak, B. Rudolf, U. Schneider, S. Curtis, D. Bolvin, A. Gruber, J. Susskind, P. Arkin, E. Nelkin 2003: The Version 2 Global Precipitation Climatology Project (GPCP) Monthly Precipitation Analysis (1979-Present). *J. Hydrometeor.*, **4**, 1147-1167.
- Aiyyer A., and J. Molinar, 2008: MJO and Tropical Cyclogenesis in the Gulf of Mexico and Eastern Pacific: Case Study and Idealized Numerical Modeling, *J. Atmos. Sci.*, **65**, 2691-2704.
- Agusti-Panareda, A., A. Beljaars, C. Cardinali, I. Genkova, C. Thorncroft, 2010: Impacts of Assimilating AMMA Soundings on ECMWF Analyses and Forecasts. *Wea. Forecasting*, **25**, 1142-1160.
- Arnault, J., F. Roux, 2009: Case study of a developing African Easterly Wave during NAMMA: An energetic point of view. *J. Atmos. Sci.*, **66**, 2991-3020.
- Asnani, G. C., 2005: *Tropical Meteorology*. Publisher: Indian Institute of Tropical Meteorology, Pashan, Pune-411008, India. 3 vols, 2241 pp.
- Barrett, B. S., and Lance M. Leslie, 2009: Links between Tropical Cyclone Activity and Madden-Julian Oscillation Phase in the North Atlantic and Northeast Pacific Basins. *Mon. Wea. Rev.*, **137**, 727-744
- Bessafi, M. and M. C. Wheeler, 2006: Modulation of south Indian Ocean tropical cyclones by the Madden-Julian oscillation and convectively coupled equatorial waves. *Mon. Wea. Rev.*, **134**, 638-656.

- Bosilovich, M. G., S.D. Schubert, M. Rienecker, R. Todling, M. Suarez, J. Bacmeister, R. Gelaro, G.-K. Kim, I. Stajner, and J. Chen, 2006: NASA's Modern Era Retrospective-analysis for Research and Applications. U.S. CLIVAR Variations, **4**, (2,) 5-8.
- , and Co-Authors, 2008: NASA's Modern Era Retrospective-analysis for Research and Applications: Integrating Earth Observations. Earthzine. Available online at: <http://www.earthzine.org/2008/09/26/nasas-modern-era-retrospective-analysis>
- Camargo, S. J., M. C. Wheeler, and A. H. Sobel, 2009: Diagnosis of the MJO Modulation of Tropical Cyclogenesis Using an Empirical Index. *J. Atmos. Sci.*, **66**, 30613074.
- Chand, S. S., and K. J. E. Walsh, 2010: The Influence of the Madden-Julian Oscillation on Tropical Cyclone Activity in the Fiji Region *J. Climate*, **23**, 868-886
- Cook, K., 1999: Generation of the African Easterly Jet and Its Role in Determining West African Precipitation. *J. Climate*, **14**, 1165-1184.
- De Felice, P, D. Monkam, A. Viltard, C. Ouss, 1990: Characteristics of North African 6-9 Day Waves during Summer 1981. *Mon. Wea. Rev.*, **118**, 2624-2633.
- , A. Viltard, and J. Oubuih, 1993: A Synoptic-Scale Wave of 6-9 Day Period in the Atlantic Tropical Troposphere during Summer 1981. *Mon. Wea. Rev.*, **121**, 1291-1298.

- Diedhiou, A., S. Janicot, A. Viltard, P. de Felice, 1998: Evidence of two regimes of easterly waves over West Africa and the tropical Atlantic. *Geophys. Res. Lett.*, **25**, 2805-2808.
- , —, —, —, H. Laurent, 1999: Easterly wave regimes and associated convection over West Africa and tropical Atlantic: results from the NCEP/NCAR and ECMWF reanalyses. *Climate Dyn.*, **15**, 795-822.
- Goldenberg, S. B., and L. J. Shapiro, 1996: Physical mechanisms for the association of El Niño and West African rainfall with Atlantic major hurricane activity. *J. Climate*, **9**, 1169-1187.
- Hall, J. D., A. J. Matthews, and D. J. Karoly, 2001: The modulation of tropical cyclone activity in the Australian region by the Madden-Julian oscillation. *Mon. Wea. Rev.*, **129**, 2970-2982.
- Hall, N. M. J., G. N. Kiladis, and C. D. Thorncroft, 2006: Three-Dimensional Structure and Dynamics of African Easterly Waves. Part II: Dynamical Modes, *J. Atmos. Sci.*, **63**, 2231-2245.
- Hopsch, S. B., C. D. Thorncroft, and K. R. Tyle, 2010: Analysis of African Easterly Waves structures and their role in influencing tropical cyclogenesis. *Mon. Wea. Rev.*, **138**, 1399-1419.
- Hsieh, J.-S., and K. Cook, 2005: Generation of African Easterly Wave disturbances: Relationship to the African Easterly Jet. *Mon. Wea. Rev.* **133**, 1311-1327.
- , and —, 2008: On the instability of the African Easterly Jet and the gen-

- eration of African Waves: reversal of the potential vorticity gradient. *J. Atmos. Sci.* **65**, 2130-2151.
- Huang, N. E., and Co-Authors, 1998: The empirical mode decomposition and the Hilbert spectrum for nonlinear and non-stationary time series analysis. *Proc. Roy. Soc. London*, **454A**, 903-995.
- , Z. Shen, and S. R. Long, 1999: A new review of nonlinear water waves - The Hilbert Spectrum. *Annu. Rev. Fluid Mech.*, **31**, 417-457.
- , and S. S. P. Shen, 2005: *Hilbert-Huang transform and its applications*. World Scientific, 311 pp.
- Janicot, S., Mounier, F., Gervois, S., Sultan, B., and Kiladis, G., 2010: The Dynamics of the West African Monsoon. Part V: The Detection and Role of the Dominant Modes of Convectively Coupled Equatorial Rossby Waves. *J. Climate*, **23**, 4005-4024.
- Kanamitsu M., W. Ebisuzaki, J. Woollen, S.-K. Yang, J. J. Hnilo, M. Fiorino, and G. L. Potter, 2002: NCEP/DOE AMIP-II Reanalysis (R-2). *Bull. Amer. Meteor. Soc.*, **83**, 1631-1643.
- Kiladis, G. N., C. D. Thorncroft, and N. M. J. Hall, 2006: Three-Dimensional Structure and Dynamics of African Easterly Waves. Part I: Observations, *J. Atmos. Sci.*, **63**, 2212-2230.
- Kistler, R., E. Kalnay, W. Collins, S. Saha, G. White, J. Woollen, M. Chelliah, W. Ebisuzaki, M. Kanamitsu, V. Kousky, H. van den Dool, R. Jenne, and M. Fiorino, 2001: The NCEP-NCAR 50-year reanalysis: Monthly means

- CD-ROM and documentation. *Bull. Amer. Meteor. Soc.*, **82**, 247–267.
- Kossin, J., S. J. Camargo, and M. Sitkowski, 2010: Climate modulation of North Atlantic hurricane tracks, *J. Climate*, **23**, 3057-3076.
- Klotzbach, P. J., 2010: On the Madden-Julian Oscillation-Atlantic hurricane relationship, *J. Climate*, **23**, 282-293.
- Kuo, H. L., 1949: Dynamic instability of two-dimensional non-divergent flow in a barotropic atmosphere. *J. Meteor.*, **6**, 105122.
- Krichak, S. O., P. Alpert, and M. Dayan, 2004: Role of atmospheric processes associated with Hurricane Olga in the December 2001 floods in Israel. *J. Hydrometeor.*, **5**, 12591270.
- Leroy, A., and M. C. Wheeler, 2008: Statistical prediction of weekly tropical cyclone activity in the southern hemisphere. *Mon. Wea. Rev.*, **136**, 3637-3654.
- Leroux, S., and N. M J. Hall, 2009: On the relationship between African Easterly Waves and the African Easterly Jet. *J. Atmos. Sci.*, **66**, 23032316.
- Madden, R. A. and P. R. Julian, 1971: Detection of a 4050-day oscillation in the zonal wind in the tropical Pacific. *J. Atmos. Sci.*, **28**, 702708.
- , and —, 1972: Description of global-scale circulation cells in the tropics with a 4050 day period. *J. Atmos. Sci.*, 29:11091123.
- Maloney, E. D., and D. L. Hartmann, 2000a: Modulation of eastern North Pacific hurricanes by the Madden-Julian oscillation. *J. Climate*, **13**, 1451-1460.

- , and —, 2000b. Modulation of hurricane activity in the Gulf of Mexico measured by the MJO. *Science*, **287**, 20022004.
- , and —, 2001: The Madden-Julian Oscillation, Barotropic Dynamics, and North Pacific Tropical Cyclone Formation. Part I: Observations *J. Atmos. Sci.* **58**, 2545-2558.
- Mounier, F., S. Janicot, G. N. Kiladis, 2007: The West African monsoon dynamics. Part III: The quasi-biweekly zonal dipole. *J. Clim.*, **21**, 1911-1928.
- Oppenheim, A. V., and R. W. Schaffer, 1975: *Digital Signal Processing*. Prentice-Hall, 585 pp.
- Onogi, K., J. Tsutsui, H. Koide, M. Sakamoto, S. Kobayashi, H. Hatsushika, T. Matsumoto, N. Yamazaki, H. Kamahori, K. Takahashi, S. Kadokura, K. Wada, K. Kato, R. Oyama, T. Ose, N. Mannoji and R. Taira, 2007: The JRA-25 Reanalysis. *J. Meteor. Soc. Japan*, **85**, 369-432.
- Parker, D. J., A. Fink, S. Janicot, J.-B. Ngamini, M. Douglas, E. Afiesimama, A. Agusti-Panared, A. Beljaars, F. Dide, A. Diedhiou, T. Lebel, J. Polcher, J.-L. Redelsperger, C. Thorncroft, and G. Ato Wilson, 2008: The AMMA radiosonde program and its implications for the future of atmospheric monitoring over Africa. *Bull. Am. Meteor. Soc.*, **89**, 1015-1027.
- Reale, O., L. Feudale and B. Turato, 2001: Evaporative moisture sources during a sequence of floods in the Mediterranean region. *Geophys. Res. Lett.*, **28**, 2085-2088.

- Rienecker, M. M., M. J. Suarez, R. Todling, J. Bacmeister, L. Takacs, H.-C. Liu, W. Gu, M. Sienkeevicz, R. D. Koster, R. Gelaro, I. Stajner, and J. E. Nielsen. The GEOS-5 Data Assimilation System. Documentation Versions 5.0.1, 5.1.0 and 5.2.0, 2008: *Technical Report Series on Global Modeling and Data Assimilation*, **27**, NASA/TM-2008-104606, 1-118. Available online at: <http://gmao.gsfc.nasa.gov/pubs/tm/>
- Shapiro, L. J., and S. B. Goldenberg, 1993: Intraseasonal oscillations over the Atlantic. *J. Climate*, **6**, 677-699.
- , and —, 1998: Atlantic Sea Surface Temperatures and Tropical Cyclone Formation. *J. Climate*, **11**, 578-590
- Thorncroft, C. D., and M. Blackburn, 1999: Maintenance of the African easterly jet *Q. J. Roy. Met. Soc.*, **125**, 763-786.
- , and B. J. Hoskins, 1994a: An idealized study of African easterly waves. Part I: A linear view. *Quart. J. Roy. Meteor. Soc.*, **120**, 953-982.
- , and —, 1994b: An idealized study of African easterly waves. Part II: A non-linear view. *Quart. J. Roy. Meteor. Soc.*, **120**, 983-1015.
- , J. Hall, and G. N. Kiladis, 2008: Three-dimensional structure and dynamics of African easterly waves. Part III: Genesis. *J. Atmos. Sci.*, **65**, 3596-3607.
- Turato, B., O. Reale, and F. Siccardi, 2004: Water vapor sources of the October 2000 Piedmont flood. *J. Hydrometeor.*, **5**, 693-712.
- Uppala, S. M., P. W. Kallberg, A. J. Simmons, U. Andrae, V. D. Bechtold et al.,

- 2005: The ERA-40 re-analysis. *Q. J. R. Meteorol. Soc.*, **131**, 2961-3012.
- Vizy, E. K. and K. H. Cook, 2009: A mechanism for African monsoon breaks: Mediterranean cold air surges. *J. Geophys. Res.*, **114**, D01104, doi:10.1029/2008JD010654.
- Wheeler, M. C., and H. H. Hendon, 2004: An all-season multivariate MJO index: development of an index for monitoring and prediction. *Mon. Wea. Rev.*, **132**, 1917-1932.
- Wu, C. M.-L., S. D. Schubert, and N. E. Huang, 1999: The development of the South Asian summer monsoon and the intraseasonal oscillation. *J. Climate*, **12**, 2054-2075.
- , —, and —, 2009a: An analysis of moisture fluxes into the gulf of California. *J. Climate*, **22**, 2216-2239.
- , Reale, O., S. Schubert, M. J. Suarez, R. Koster, P. Pegion, 2009b: African Easterly Jet: Structure and Maintenance. *J. Climate*, **22**, 4459-4480.
- Yanai, M. and M. Murakami, 1970: Spectrum analysis of symmetric and anti-symmetric equatorial waves. *J. Meteor. Soc. Japan*, **48**, 331-346.

## List of Figures

1	JAS zonal wind climatology ( $m s^{-1}$ , shaded, 1980-2001) at 600 hPa based on MERRA, ERA-40, NCEP-R2, JRA-25, of $K(y)$ , ( $10^{-11}m^{-1}s^{-1}$ , contours at +/- .5,1,2,3,5 (left column), and $-\partial u/\partial y$ ( $10^{-6}s^{-1}$ , contours at +/-1,5,10,15,20, right column). The areas where vorticity is positive are shaded in white in the left column. . . . .	42
2	Vertical meridional cross-section at $0^\circ$ of JAS zonal wind climatology ( $m s^{-1}$ , shaded, 1980-2001) based on MERRA, ERA-40, NCEP-R2, JRA-25, of $K(y)$ , ( $10^{-11}m^{-1}s^{-1}$ , contours at +/- .5,1,2,3,5 (left column), and $-\partial u/\partial y$ ( $10^{-6}s^{-1}$ , contours at +/-1,5,10,15,20, right column). . . . .	43
3	Vertical meridional cross-section at $20^\circ W$ of JAS zonal wind climatology ( $m s^{-1}$ , shaded, 1980-2001) based on MERRA, ERA-40, NCEP-R2, JRA-25, of $K(y)$ , ( $10^{-11}m^{-1}s^{-1}$ , contours at +/- .5,1,2,3,5 (left column), and $-\partial u/\partial y$ ( $10^{-6}s^{-1}$ , contours at +/-1,5,10,15,20, right column). . . . .	44
4	JAS precipitation ( $mm d^{-1}$ , left column, upper color bar) and departure from the GPCP (right panels, lower color bar). . . . .	45
5	First and second EOFs of the meridional component of the 700hPa wind, computed during JAS, in neutral ENSO years, from $40^\circ W$ to $10^\circ E$ and $10^\circ N$ to $20^\circ N$ . . . . .	46

6	Hilbert-Huang (left) and Fourier (right) spectra based on MERRA meridional 700 hPa wind (full field) at one single point ( $17^{\circ}W$ and $12^{\circ}N$ , JAS, 1980-2001). . . . .	47
7	Hilbert-Huang (left) and Fourier (right) spectra based on MERRA meridional 700 hPa wind (full field) at one single point ( $5^{\circ}W$ and $26^{\circ}N$ , JAS, 1980-2001). . . . .	48
8	Variance of the 6-hourly meridional component of the wind, bandpass filtered through a 2.5-6 day passband ([units] left column, upper color bar) and fraction of the total (right panels, lower color bar). The shading indicates the area where the necessary condition for barotropic instability, computed as in Fig. 1, (with $K$ in the range $-/+ 10^{-11}$ ), is satisfied.	49
9	Variance of 6-hourly precipitation, bandpass filtered through a 2.5-6 day passband ([units] left column, upper color bar) and fraction of the total (right panels, lower color bar). . . . .	50
10	Variance of 6-hourly zonal (left panels, upper color bar) and meridional (right panels, lower color bar) wind, bandpass filtered through a 2.5-6 day passband ( $(ms^{-1})^2$ ), from MERRA analyses. . . . .	51
11	Variance of 6-hourly zonal (left panels, upper color bar) and meridional (right panels, lower color bar) wind, bandpass filtered through a 6-9 day passband ( $(ms^{-1})^2$ ), from MERRA analyses. . . . .	52

12	Variance of: hourly meridional wind (upper panel, left color bar) filtered through a 2.5-9 day (upper panel, left color bar), 6-9 day (central panel, central color bar), and 2.5-6 day (lower panel, right color bar) passband ( $(ms^{-1})^2$ ), from MERRA analyses. . . . .	53
13	Lag correlation coefficient of 700hPa meridional (left) and zonal (right) wind computed for $20^{\circ}W$ and $26^{\circ}N$ (shaded) and streamline of total wind, filtered through a 6-9 passband, from MERRA analyses. . . . .	54
14	JAS zonal wind climatology ( $m s^{-1}$ , shaded, both columns, upper and central panels), and cross section (lower panels). Variance of the 6-hourly meridional component of the wind, bandpass filtered through a 2.5-6 day passband ([units] left column, red contour) and $-\partial u/\partial y$ (right panels, lower color bar). The variance is plotted only in the areas where the necessary condition for barotropic instability, computed as in Fig. 1, (with $K$ in the range $-/+ 10^{-11}$ ), is satisfied. The red dots in the upper right panel indicate observed cyclogenesis. . . . .	55

Climatology of AEJ (shaded),  $K(y)$  (contour), and  $-d[u]/dy$  (contour)  
(1980–2001)

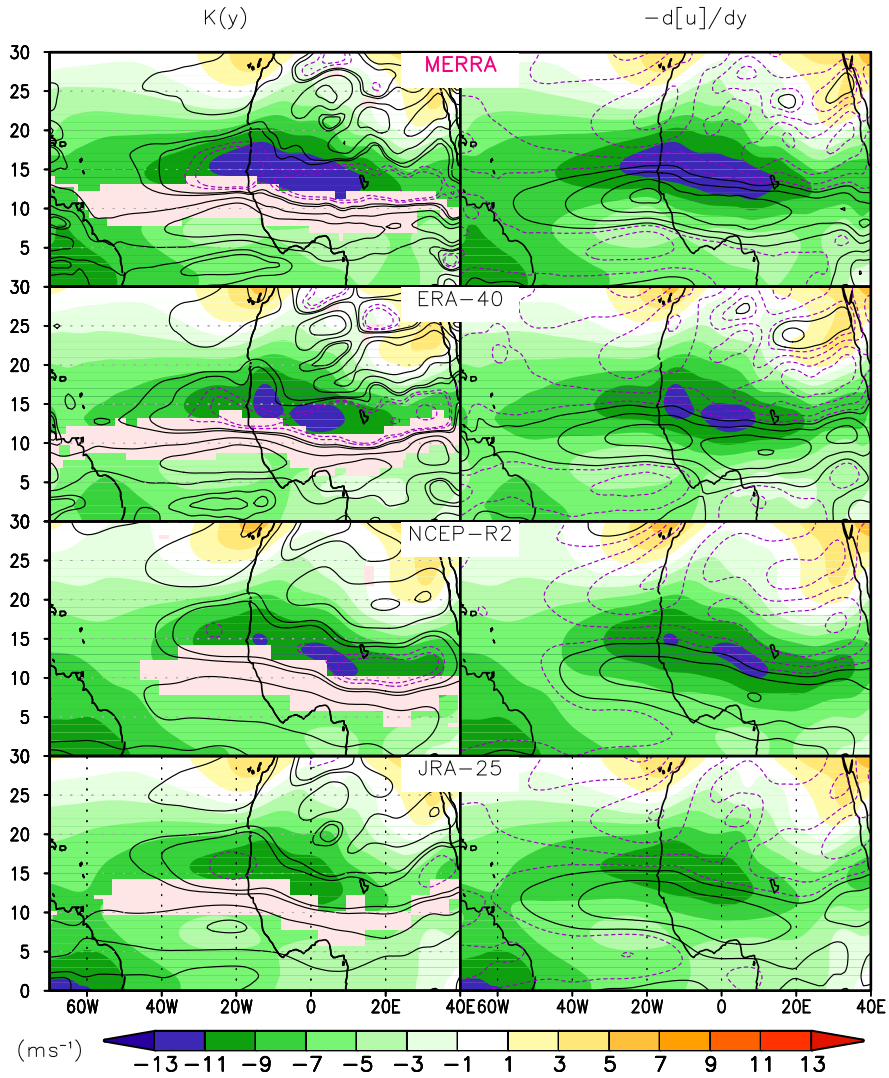


Figure 1: JAS zonal wind climatology ( $m s^{-1}$ , shaded, 1980-2001) at 600 hPa based on MERRA, ERA-40, NCEP-R2, JRA-25, of  $K(y)$ , ( $10^{-11} m^{-1} s^{-1}$ , contours at  $\pm 0.5, 1, 2, 3, 5$ ) (left column), and  $-\partial u / \partial y$  ( $10^{-6} s^{-1}$ , contours at  $\pm 1, 5, 10, 15, 20$ ) (right column). The areas where vorticity is positive are shaded in white in the left column.

Climatology of AEJ (shaded), and  $K(y)$  and  $dudy$  (contour) at 0-deg Longitude (1980–2001)

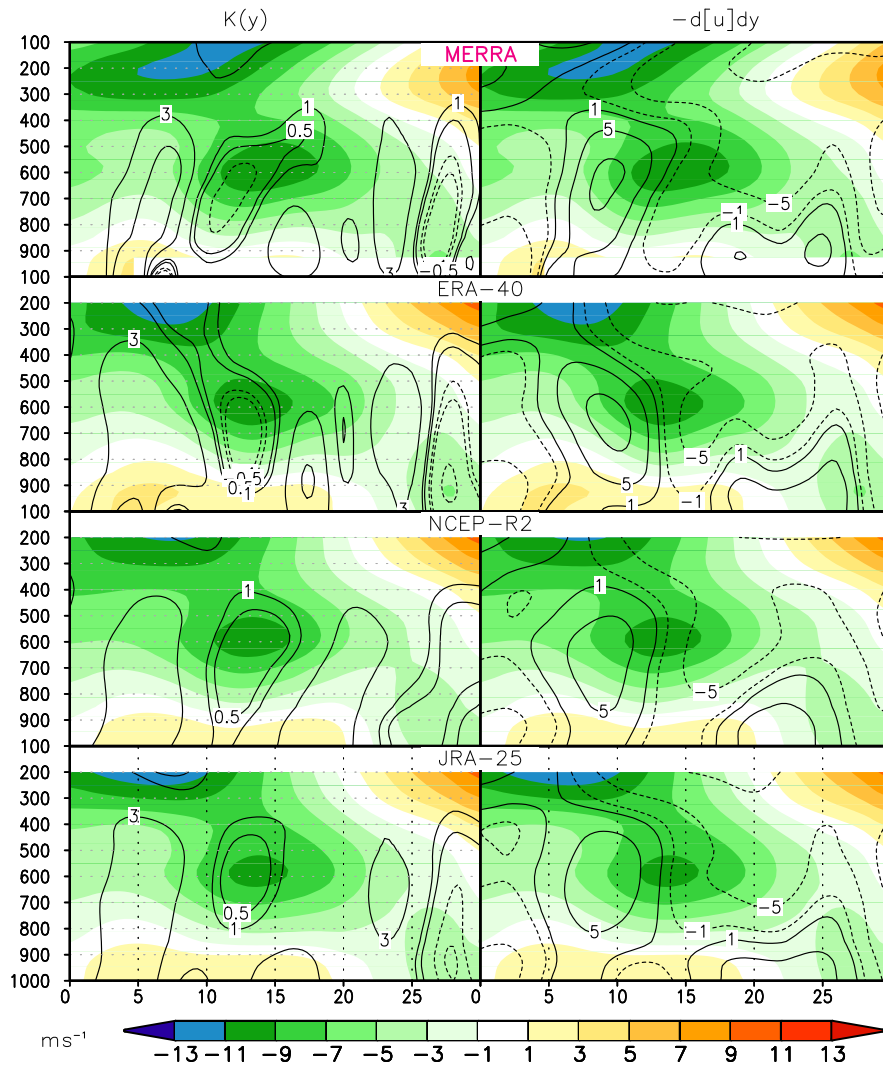


Figure 2: Vertical meridional cross-section at  $0^\circ$  of JAS zonal wind climatology ( $m s^{-1}$ , shaded, 1980-2001) based on MERRA, ERA-40, NCEP-R2, JRA-25, of  $K(y)$ , ( $10^{-11} m^{-1} s^{-1}$ , contours at  $\pm .5, 1, 2, 3, 5$  (left column), and  $-\partial u / \partial y$  ( $10^{-6} s^{-1}$ , contours at  $\pm 1, 5, 10, 15, 20$ , right column).

Climatology of AEJ (shaded), and  $K(y)$  and  $-d[u]/dy$  (contour) at  $20^{\circ}W$  (1980–2001)

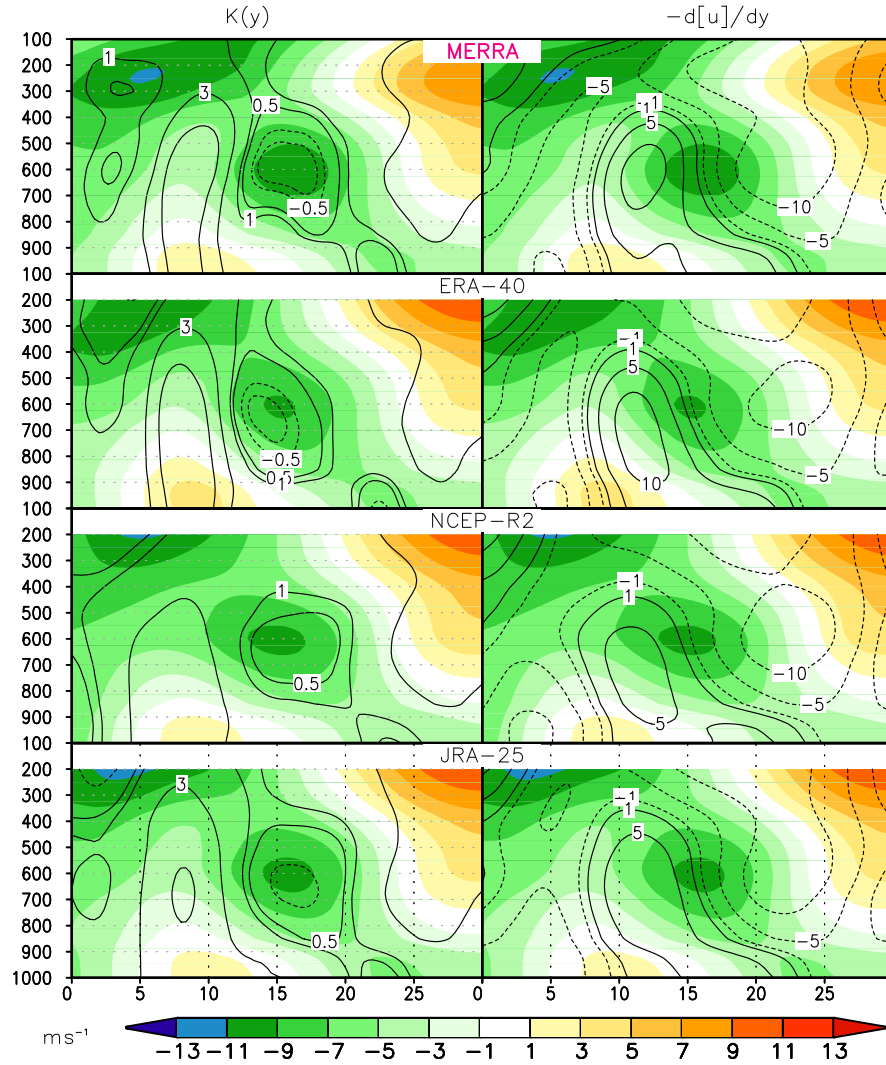


Figure 3: Vertical meridional cross-section at  $20^{\circ}W$  of JAS zonal wind climatology ( $m s^{-1}$ , shaded, 1980-2001) based on MERRA, ERA-40, NCEP-R2, JRA-25, of  $K(y)$ , ( $10^{-11} m^{-1} s^{-1}$ , contours at  $\pm .5, 1, 2, 3, 5$  (left column), and  $-\partial u/\partial y$  ( $10^{-6} s^{-1}$ , contours at  $\pm 1, 5, 10, 15, 20$ , right column).

Precipitation Climatology (1980–2001)

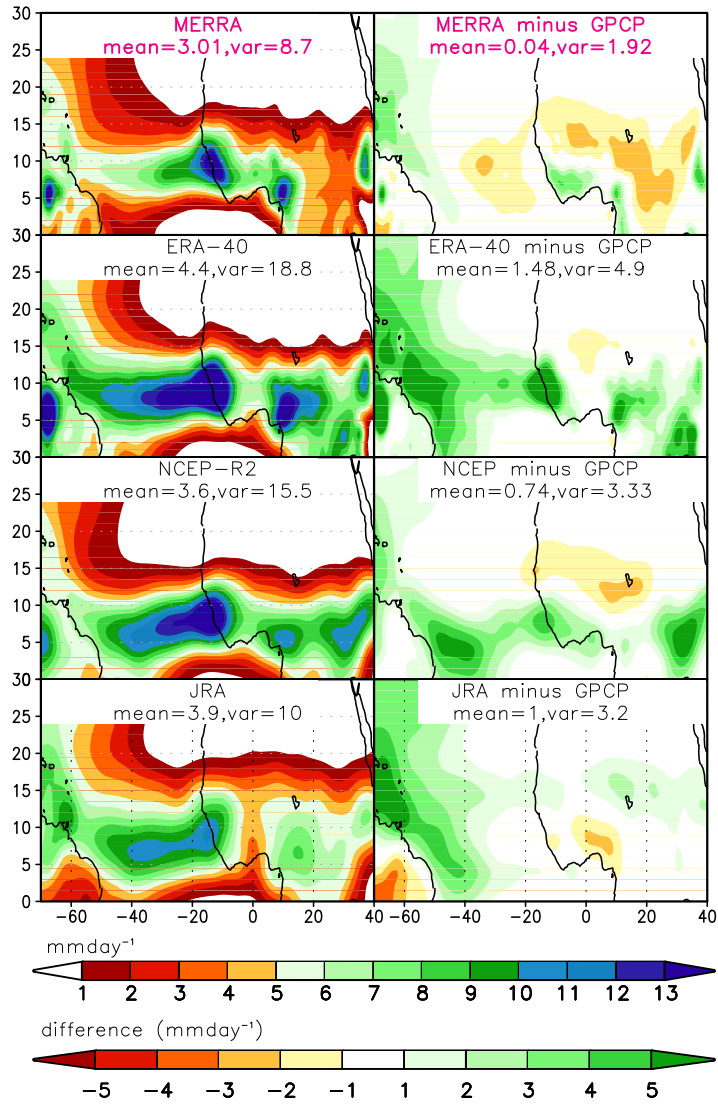


Figure 4: JAS precipitation ( $\text{mm d}^{-1}$ , left column, upper color bar) and departure from the GPCP (right panels, lower color bar).

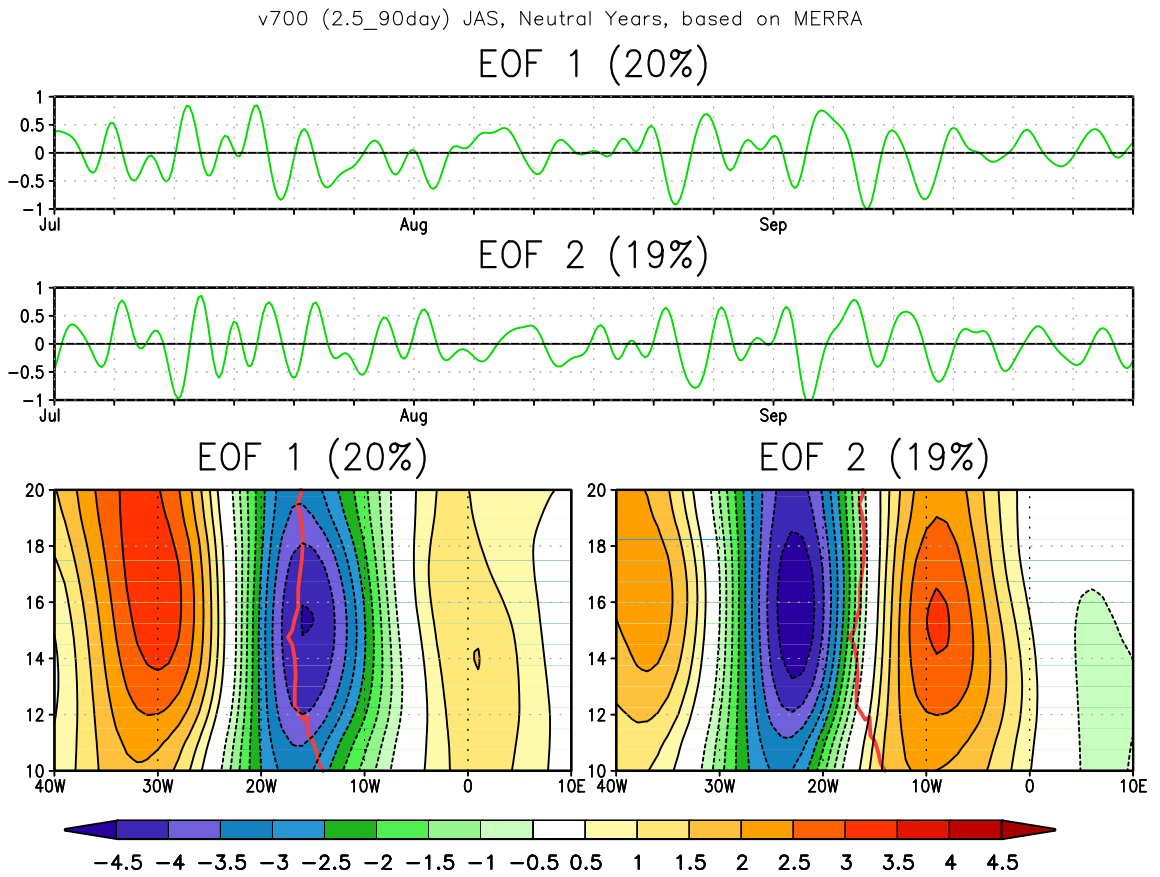


Figure 5: First and second EOFs of the meridional component of the 700hPa wind, computed during JAS, in neutral ENSO years, from  $40^{\circ}W$  to  $10^{\circ}E$  and  $10^{\circ}N$  to  $20^{\circ}N$ .

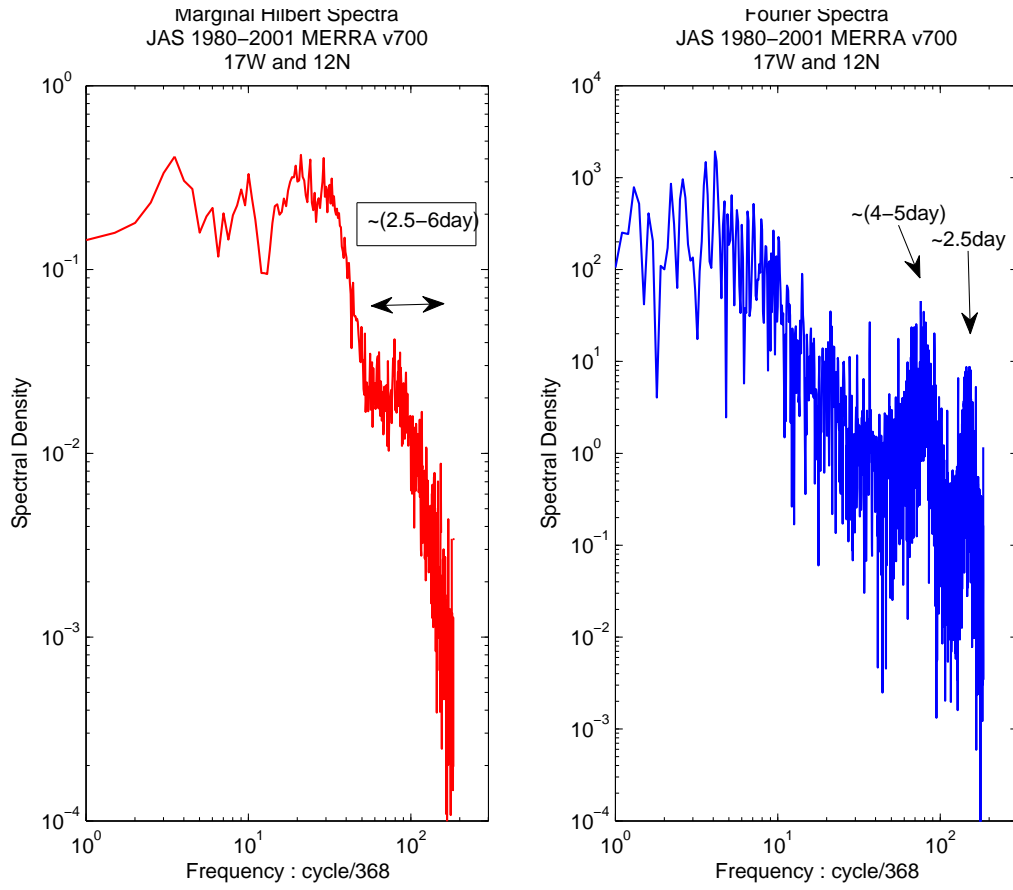


Figure 6: Hilbert-Huang (left) and Fourier (right) spectra based on MERRA meridional 700 hPa wind (full field) at one single point ( $17^{\circ}W$  and  $12^{\circ}N$ , JAS, 1980-2001).

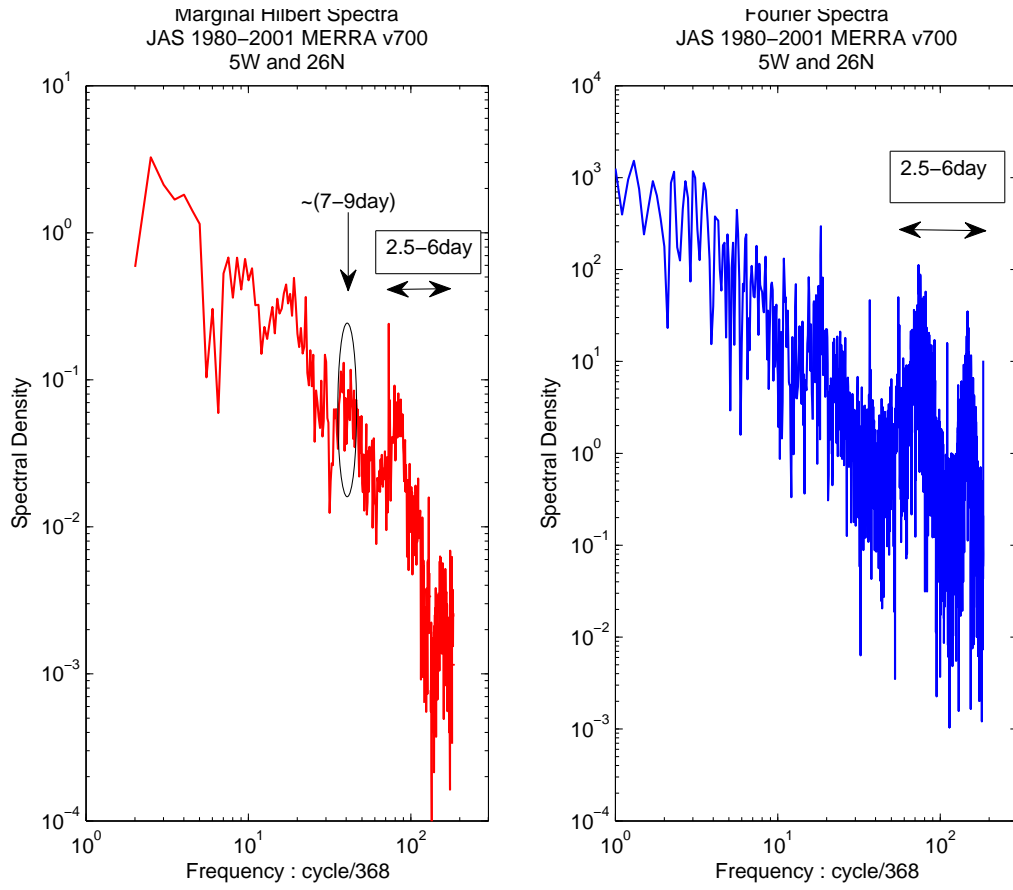


Figure 7: Hilbert-Huang (left) and Fourier (right) spectra based on MERRA meridional 700 hPa wind (full field) at one single point ( $5^{\circ}W$  and  $26^{\circ}N$ , JAS, 1980-2001).

Climatology of v700 Variance (1980–2001)

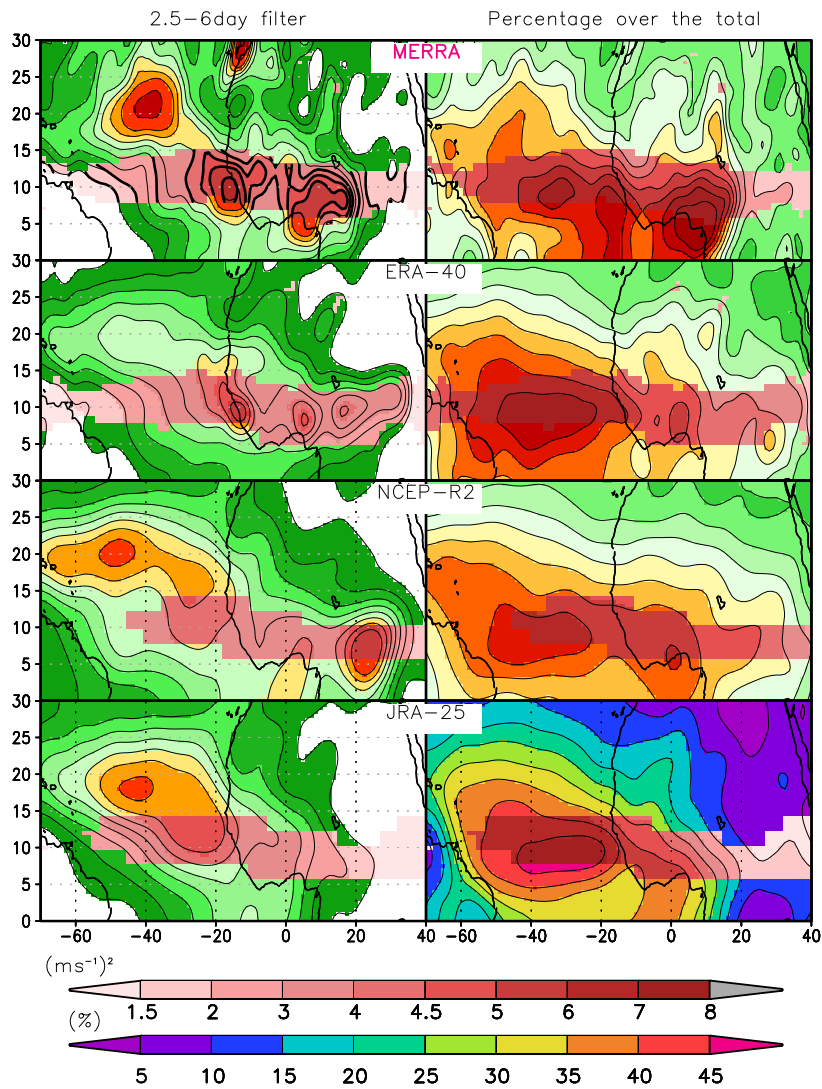


Figure 8: Variance of the 6-hourly meridional component of the wind, bandpass filtered through a 2.5-6 day passband ([units] left column, upper color bar) and fraction of the total (right panels, lower color bar). The shading indicates the area where the necessary condition for barotropic instability, computed as in Fig. 1, (with  $K$  in the range  $-/+ 10^{-11}$ ), is satisfied.

Climatology of Precipitation Variance (1980–2001)

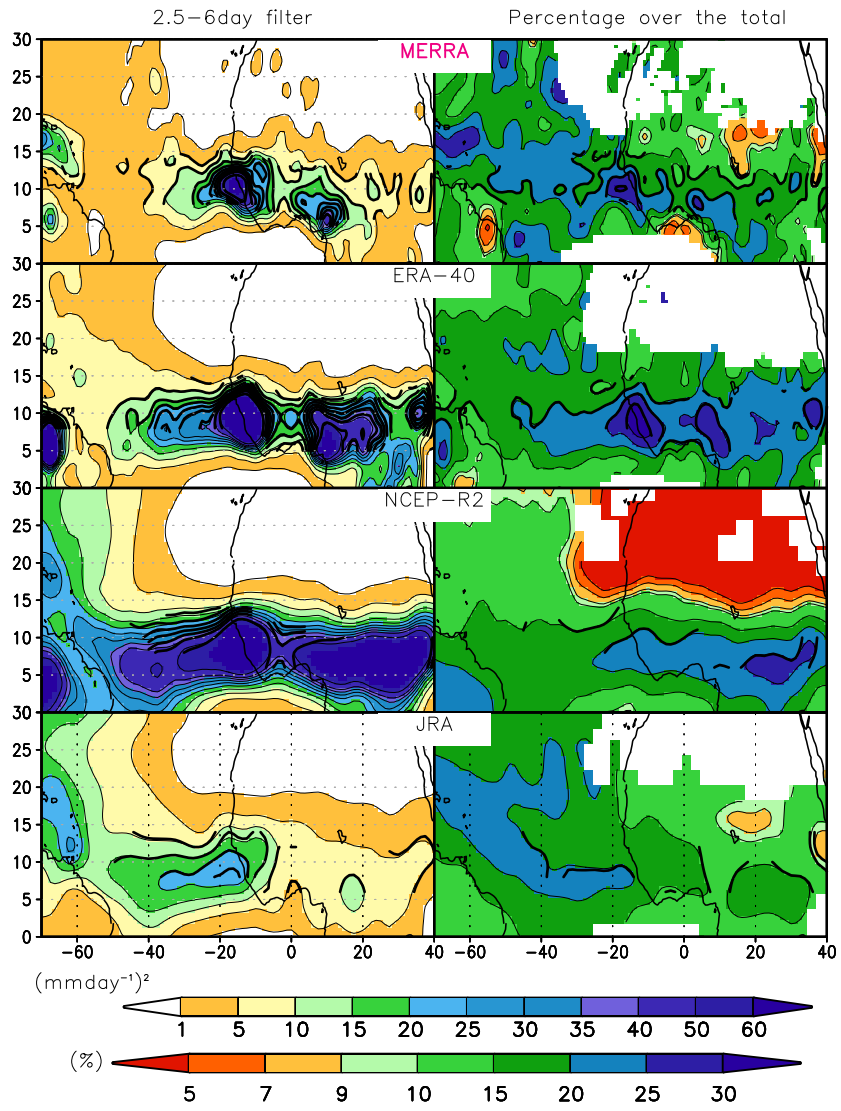


Figure 9: Variance of 6-hourly precipitation, bandpass filtered through a 2.5-6 day pass-band ([units] left column, upper color bar) and fraction of the total (right panels, lower color bar).

Variance (2.5\_6day) Based on MERRA (1980–2001)

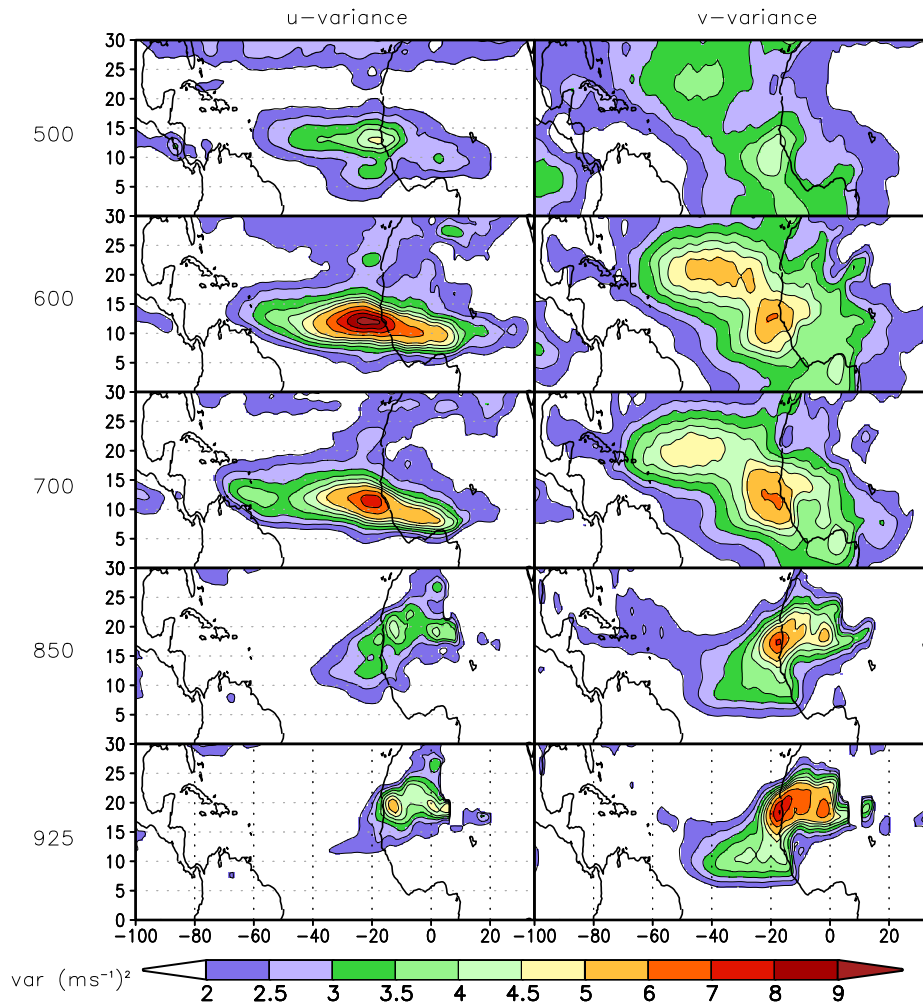


Figure 10: Variance of 6-hourly zonal (left panels, upper color bar) and meridional (right panels, lower color bar) wind, bandpass filtered through a 2.5-6 day passband  $((ms^{-1})^2)$ , from MERRA analyses.

Variance (06\_09day) Based on MERRA (1980–2001)

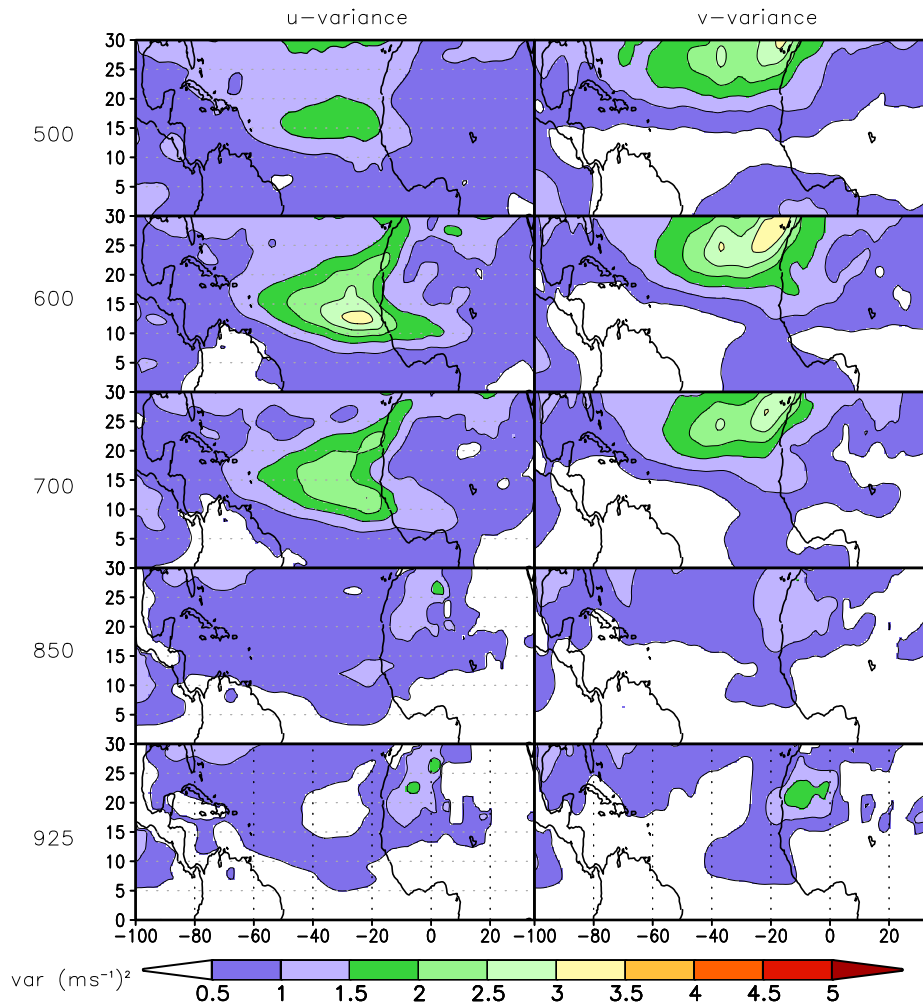


Figure 11: Variance of 6-hourly zonal (left panels, upper color bar) and meridional (right panels, lower color bar) wind, bandpass filtered through a 6-9 day passband  $((ms^{-1})^2)$ , from MERRA analyses.

Climatology of v-variance ( $\text{ms}^{-1}$ )<sup>2</sup> (1980–2001)

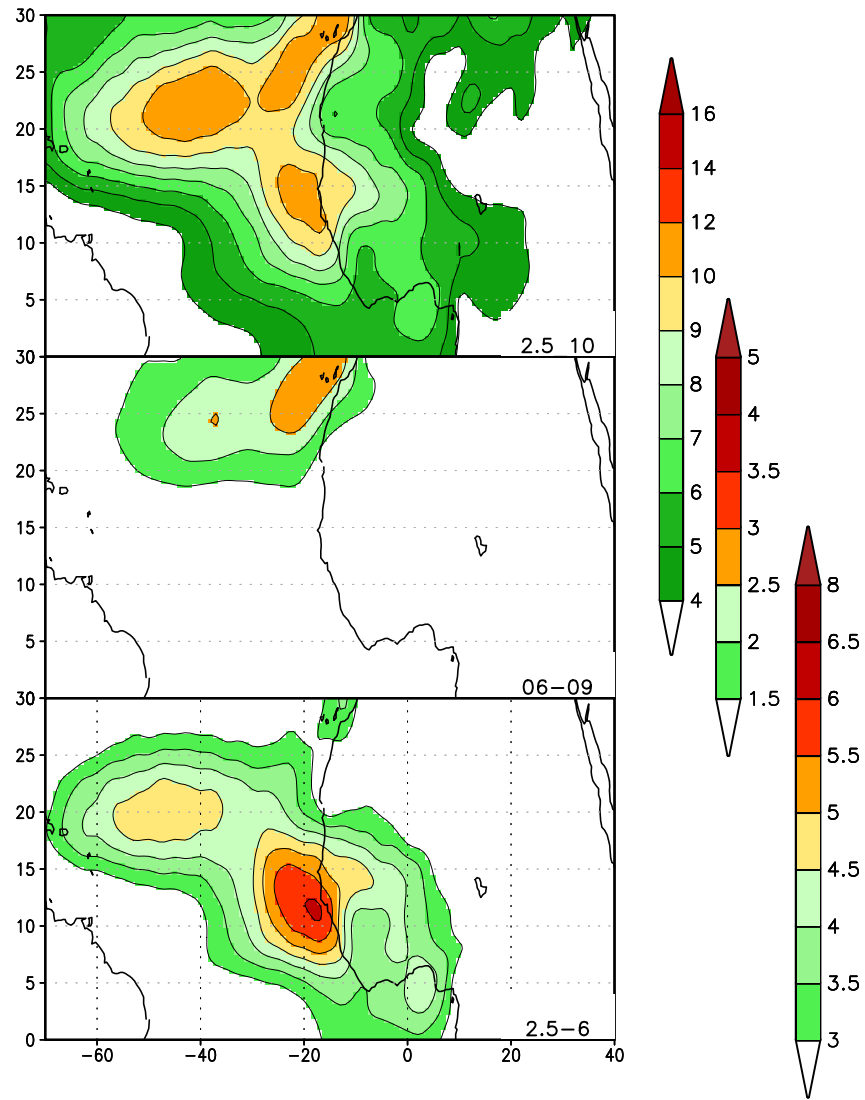


Figure 12: Variance of: hourly meridional wind (upper panel, left color bar) filtered through a 2.5-9 day (upper panel, left color bar), 6-9 day (central panel, central color bar), and 2.5-6 day (lower panel, right color bar) passband ( $(\text{ms}^{-1})^2$ ), from MERRA analyses.

Lag Correlation Coefficient between v700 and u and v  
 Location of v700 index at 20W and 26N; all data in 06\_09day  
 streamline of u and v

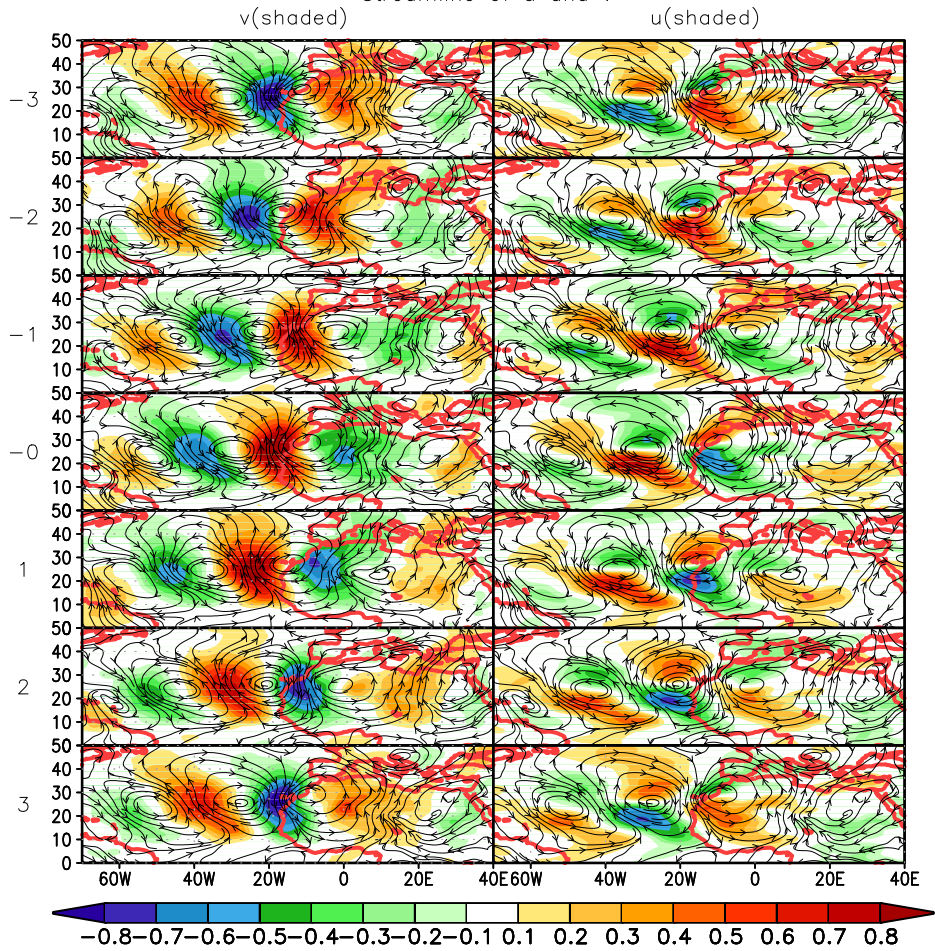


Figure 13: Lag correlation coefficient of 700hPa meridional (left) and zonal (right) wind computed for  $20^{\circ}W$  and  $26^{\circ}N$  (shaded) and streamline of total wind, filtered through a 6-9 passband, from MERRA analyses.

Zonal Wind Climatology for JAS Based on MERRA (1980–2001)  
 Neutral (1980,81,83,84,85,89,95,96,00,01); Zonal Wind (shaded)

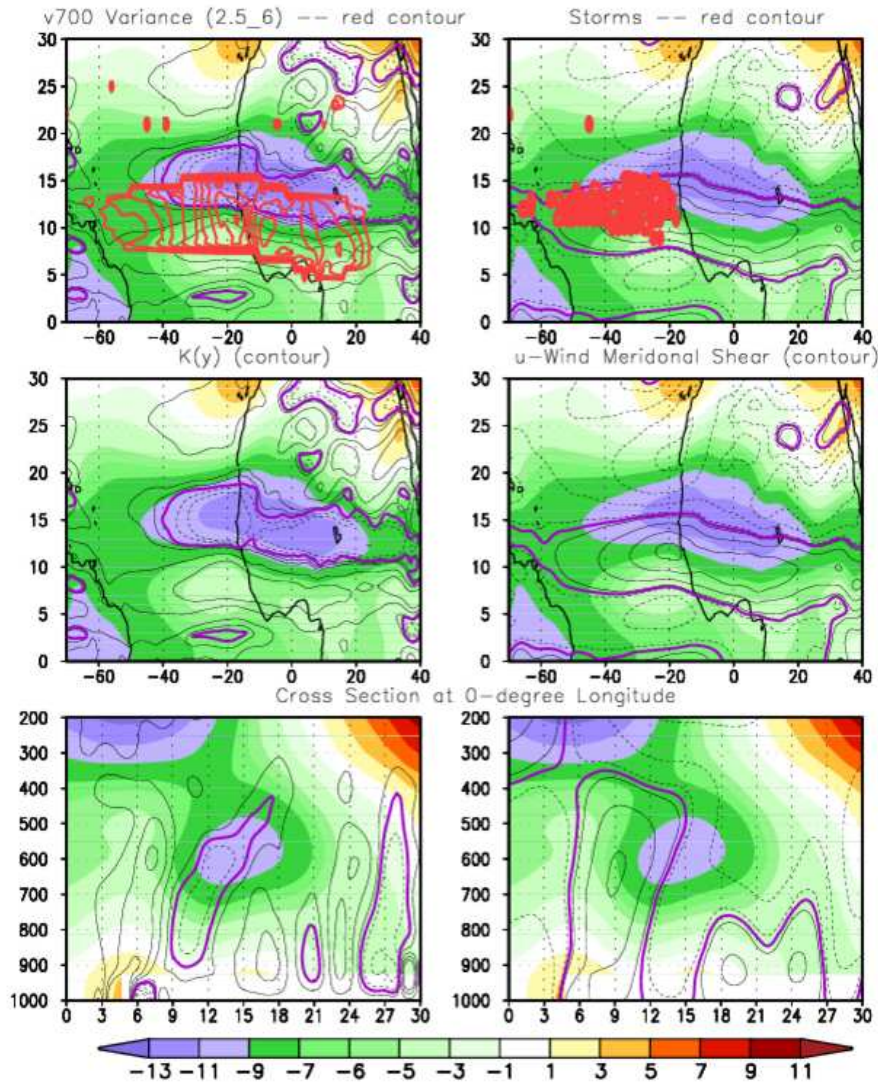


Figure 14: JAS zonal wind climatology ( $m s^{-1}$ , shaded, both columns, upper and central panels), and cross section (lower panels). Variance of the 6-hourly meridional component of the wind, bandpass filtered through a 2.5-6 day passband ([units] left column, red contour) and  $-\partial u/\partial y$  (right panels, lower color bar). The variance is plotted only in the areas where the necessary condition for barotropic instability, computed as in Fig. 1, (with  $K$  in the range  $-/+ 10^{-11}$ ), is satisfied. The red dots in the upper right panel indicate observed cyclogenesis.